



POLITECNICO

MILANO 1863

Prova finale di Propulsione Aerospaziale

Preliminary Study of an Ariane 5 ECA and JWST Propulsion System

A.A.: 2022-2023

Prof: Galfetti Luciano

Garghetti Andrea	10734647	Melchiorre Federico	10710428
Grandinetti Roberta	10713569	Miccoli Francesco Antonio	10782473
Juvara Matteo Giovanni	10726898	Miolo Tommaso	10755151
Marzolini Alessandra	10724764	Modelli Simone	10728962
Mazzotti Luca	10744992	Nuccio Gabriele	10730683



Contents

Acronyms	4
Introduction	4
1 General Architecture	7
1.1 Lower composite	7
1.2 Upper composite and supporting structure	9
1.3 Fairing and Sylfa 5	10
2 EAP: Etage d'Accélération à Poudre	12
2.1 Characterization of the stage	12
2.1.1 Characterization of the Propellant	13
2.2 Modelling of the engine	14
2.2.1 Index of symbols and constant values	14
2.2.2 CEA analysis	15
2.2.3 Data Analysis	16
2.3 Grain configuration analysis	18
2.3.1 Hypothesis	18
2.3.2 Round port grain	19
2.3.2.1 Geometry	19
2.3.2.2 Performance	20
2.3.3 Star Grain	21
2.3.3.1 Geometry	21
2.3.3.2 Performance	23
2.3.4 Moonburn	24
2.3.4.1 Geometry	24
2.3.4.2 Performance	26
2.3.5 Conclusion	27
2.4 Performance - other parameters	27
2.4.1 Coefficient of thrust and characteristic velocity	27
2.4.2 Specific impulse	28
2.4.3 Total and volumetric impulse	29
2.5 Nozzle Dimensioning	29
3 EPC: Etage Principal Cryotechnique	31
3.1 Characterization of the Stage	32
3.1.1 Characterization of the propellant	33
3.1.1.1 Liquid Oxygen	33
3.1.1.2 Liquid Hydrogen	33
3.1.2 Engine description: Vulcan 2 Engine	34
3.1.3 Operational data	36
3.2 Modelling of the engine	36
3.2.1 Index of variable and constants	37



3.2.2	Hypothesis for the calculations	39
3.2.3	CEA analysis	39
3.2.4	Nozzle Dimensioning	40
3.2.5	Performances	42
3.2.5.1	Thrust	42
3.2.5.2	Thrust coefficient	42
3.2.5.3	Specific Impulse	43
3.2.5.4	Volumetric Impulse	43
3.2.5.5	Mach number	44
3.2.6	Combustion chamber and Injection Plate	45
3.2.6.1	Combustion chamber Dimensioning	45
3.2.6.2	Injection plate	45
3.2.7	Shear Coaxial Injectors	48
3.2.8	Helium Pressurization System	50
3.2.8.1	Turbopump system	52
3.3	Cooling system	55
3.3.1	Regenerative cooling	55
3.3.1.1	Heat flux from the wall to the coolant flow	56
3.3.1.2	Heat flux through the wall	56
3.3.1.3	Convective wall heat	57
3.3.1.4	Balance solution	57
3.3.1.5	Film cooling	58
4	James Webb Space Telescope	61
4.1	Characterization of the stage	62
4.1.1	Characteristics	62
4.1.2	Introduction	62
4.2	Characterization of the propellant	63
4.2.1	Hydrazine	63
4.2.2	Dinitrogen Tetroxide	64
4.3	Secondary combustion augmented thrust	64
4.4	Dual Thruster Module	65
4.5	Monopropellant Catalyst Thrusters	65
4.5.1	Start Transient	66
4.5.2	Catalyst Bed Lifetime	68
4.5.3	Heat Transfer to the Feed System	68
A	MATLAB Codes	A2
A.1	Solid Propellant	A2
A.1.1	CEAm analysis	A2
A.1.2	Grains configurations	A4
A.1.3	Nozzle dimensioning	A9
A.2	Liquid Propellant	A9
A.2.1	Liquid 1	A9
A.2.2	Liquid 2	A12



Acronyms

Al Aluminium	LOX Liquid Oxygen
CEA Chemical Equilibrium Application	MCC Mid-course Corrections
CEAm Chemical Equilibrium Application for MatLab	MON Mixed Oxides of Nitrogen
DTMs Dual Thrusters Modules	MRE Monopropellant Rocket Engines
EAP Etage d'Accélération à Poudre	N2H4 Hydrazine
ECA Evolved Cryogenic model A	N2O4 Dinitrogen Tetroxide
EPC Etage Principal Cryotechnique	NASA National Aeronautics and Space Administration
ESC-A Etage Supérieur Cryotechnique de type A	NH4ClO4 Ammonium Perchlorate
gHe Gaseous Helium	NTO Nitrogen Tetroxide
GTO Geostationary Transfer Orbit	OTE Optical Telescope Element
HTPB hydroxyl-terminated polybutadiene	SCAT Secondary Combustion Augmented Thruster
ISIM Integrated Science Instrument Module	TEG Turbine Exhaust Gases
JWST James Webb Space Telescope	UPG Guiana Propellant Plant
LH2 Liquid Hydrogen	VEB Vehicle Equipment Bay



Introduction



Figure 1: James Webb launch with an Ariane 5 ECA [12]

Rockets have revolutionised the way we explore space and have enabled us to reach new heights in our understanding of the universe. The development of powerful and efficient rocket technology has made it possible to launch spacecraft into orbit, land on other planets, and study the cosmos in ways that were once unimaginable.

One of the most significant players in the rocketry field is the Ariane 5 launcher, a heavy-weight rocket that has been instrumental in launching numerous missions into space. The Ariane 5 launcher is a European launch vehicle that was designed to carry heavy payloads into space, such as large communication satellites and scientific instruments. The rocket is known for its reliability, having completed over 100 successful launches since its first flight in 1996.

As we continue to explore the vast frontier of space, the Ariane 5 launcher will undoubtedly remain a vital tool in our quest for knowledge and discovery. The Ariane 5 launcher has been upgraded in successive versions: G, G+, GS, ECA and ES ATV version. ESA's Ariane 5 ECA (Evolved Cryogenic, model A), manufactured by ArianeGroup, has completed 80 successful launches from Europe's Spaceport in French Guiana since 2002.

It is designed to deliver payloads, mainly communications satellites, with a mass of more than 10t into geostationary transfer orbit (GTO), including the supporting structure and adaptors. The Ariane 5 ECA can launch one, two or three very large satellites. A dual launch configuration is the most commonly used. Owing to its performance and flexibility to adapt to different missions requirements, Ariane 5 ECA is also used by institutional customers for non-GTO missions.

On December 25, 2021, Ariane 5 launched the James Webb Space Telescope on its way to orbit in the Sun-Earth L2 Lagrange Point.



The scope of this document is to thoroughly analyze Ariane 5's lower composite, EAP and EPC, from a propulsive perspective, and to briefly examine James Webb's propulsion system.

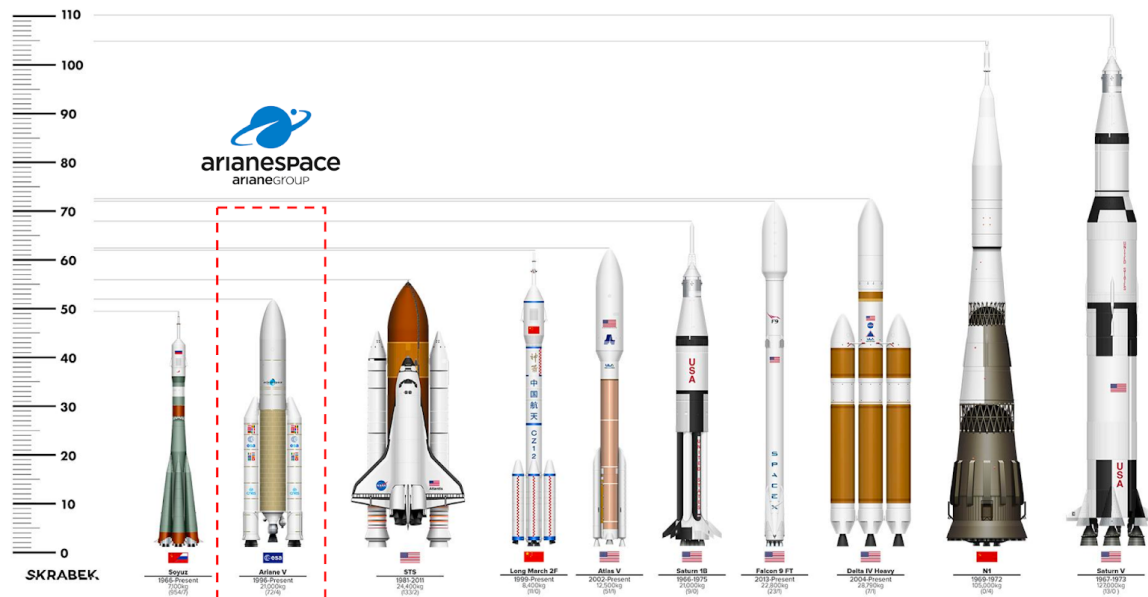


Figure 2: Ariane 5 size comparison



1 General Architecture

The launch vehicle configuration consists of three parts [9]:

- Lower Composite
- Upper Composite
- Fairing and Sylde 5

This chapter will provide a general overview of the Architecture of the launcher, explaining the general characteristics of every stage.



Figure 1.1: Ariane 5 ECA exploded diagram

1.1 Lower composite



Figure 1.2: Detail of the Lower Composite at the launch site [9]

The lower composite comprises 2 elements:



- The Etage d'Accélération à Poudre (EAP) consists of 2 boosters: they are 3 m diameter, 31 m high, and carry 240 t of solid propellant each, together they provide 1200 t of thrust at liftoff. The maximum thrust during flight can reach 1300 t. Time of burn for the EAP burns is about 135 s. After separating from the main stage the boosters re-enter the atmosphere above the Atlantic Ocean.
- Etage Principal Cryotechnique (EPC) (cryogenic main core stage) is 5.4 m in diameter and 30 m in height, it contains 175 t of propellants (25 t of liquid hydrogen and 150 t of liquid oxygen), and is equipped with one Vulcain 2 engine that provides 136 t of thrust. EPC operation time is about 540 s. It also provides roll control during the main propulsion phase. At shut down, EPC separates from the upper composite at an altitude between 160 km and 210 km, depending on the mission's trajectory, and performs a destructive reentry in the atmosphere over the Atlantic Ocean.

Total liftoff thrust is about 1340 t.

During the launch sequence the Vulcain 2 engine is fired first and left to reach its nominal operating level. The process usually takes few seconds. After the engine reaches its nominal operating level, the two solid-propellant boosters are fired.



1.2 Upper composite and supporting structure



Figure 1.3: Ariane 5 ECA Upper Stage for the Space Webb telescope before integration [11]

The upper composite comprises 3 elements:

- The cryogenic upper stage (Etage Supérieur Cryotechnique de type A (ESC-A)) houses 17.4 t of propellant (LH₂ and LOX) and the HM7B engine, that is reused from Ariane 4's third stage. The HM7B operates for about 945 s, provides 6.5 t of thrust and attitude control during the propulsion phase and the separation sequences of the payloads.
- The Vehicle Equipment Bay (VEB)-C autonomously controls the whole vehicle. Its structure is made of composite material. The VEB transmits all key flight parameters to the ground station network.
- The supporting structure is a conical adaptor that is mounted on top of the VEB and provides the standard 2624 mm diameter interface with the payload adaptor.

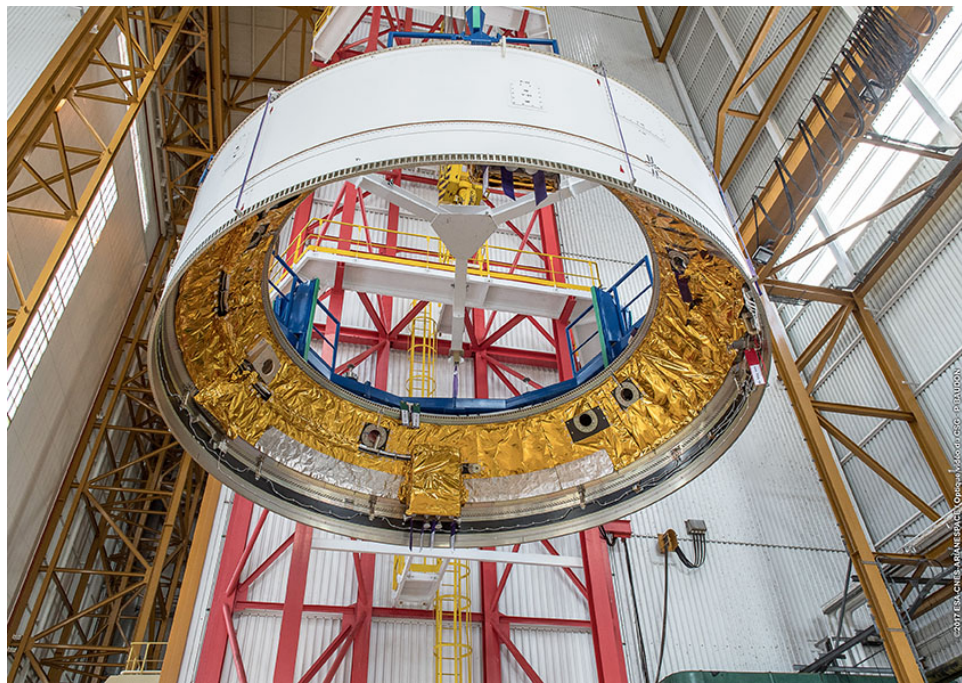


Figure 1.4: VEB during integration phase

1.3 Fairing and Sylda 5



Figure 1.5: Fairing of the Ariane 5 for Galileo Mission [4]

The launcher upper part comprises 2 elements:

- The fairing protects the payload at liftoff and during atmospheric flight (5.4 m diameter)



ter, 17 m high). It is split by two pyrotechnical commands and jettisoned more than 3 minutes after liftoff, at an altitude above 100 km.

- The Sylde 5 (Système de Lancement Double Ariane 5) structure accommodates the lower and upper satellites and is available in six different models : 4.6 m diameter and height varies from $4.9 \div 6.4m$ in increments of 0.3 m. Due to the size of the JWST and the nature of the mission the Sylde 5 structure was not necessary during the launch of the JWST.



Figure 1.6: Sylde Structure before integration (not used in James Webb launch) [4]



2 EAP: Etage d'Accélération à Poudre

2.1 Characterization of the stage



Figure 2.1: EAP being transported to the assembling facility [4]

In this section a thorough analysis of the Etage d'Accélération à Poudre (EAP) solid boosters will be carried out.

Each EAP is 31 meters high and 3 meters in diameter, weights 37t when empty and contains about 230 t of solid propellant. They provide roughly 92% of the total thrust at lift off, each giving up to 6470 kN of thrust with a specific impulse of 275 s and a burning time of 135 s.

They are equipped with parachutes in order to recover them from the Atlantic Ocean. At the base of each booster is the 3.8 m long solid rocket engine nozzle. Thanks to hydraulically-controlled servo actuators it can be swiveled up to 7.3 deg around its axis to vary the direction of thrust and to provide flight control. The outer diameter of the nozzle

is 3.1 m.

The booster stage's solid rocket motor is made up of three segments of propellant grains (S1, S2, S3) enclosed by a steel casing and joined together. The first segment is loaded with 23.5 t of propellant in Colleferro (Italy), while the middle and bottom segments are filled in the solid propellant production plant (UPG) at the Spaceport. The middle segment contains 107.5 t of propellant and the bottom segment contains 107 t of propellant. Although the casings are only 8 mm thick, they can resist pressures of up to 64 bar.

A propellant mix of 68% ammonium perchlorate (oxidizer), 18% aluminum (fuel), and 14% polybutadiene (binder) is used in the solid rocket motors. The combustion process is initiated by a pyrotechnic device: it takes 350 ms for the igniter in the upper segment of the booster to ignite the propellant. The radial rate of combustion, from the center outward, is approximately 7.4 mm/s.

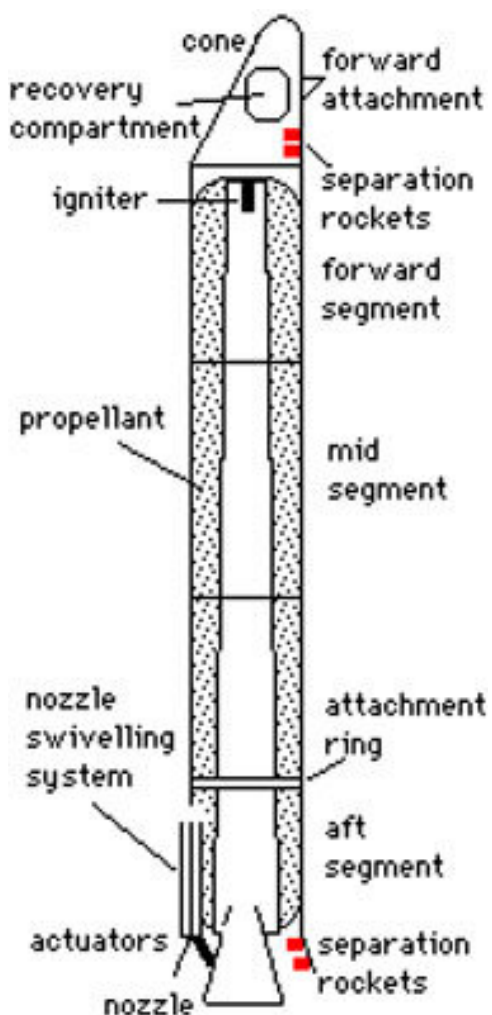


Figure 2.2: EAP solid rocket booster breakdown [10]

2.1.1 Characterization of the Propellant

The solid propellant composed of Ammonium Perchlorate (NH_4ClO_4) (68%), Aluminium (Al) (18%), and hydroxyl-terminated polybutadiene (HTPB) (14%) exhibits several distinct properties that contribute to its effectiveness as a propulsive material [1].



- NH₄ClO₄ serves as the oxidizer in the propellant mixture. It possesses high oxygen content, which facilitates the combustion process and supports the release of a substantial amount of energy .
- Aluminium acts as the fuel component and contributes to the overall energy output of the propellant. Its high heat of combustion and reactivity with the oxidizer enhance the propellant's performance.
- HTPB acts as the binder and providing structural integrity to the propellant. HTPB also contributes to the overall energy content and regulates the the burning rate of the propellant.

This combination of ingredients results in a solid propellant with excellent energy output, stability, and controllable combustion characteristics, making it suitable for various propulsion applications.

2.2 Modelling of the engine

The current section goes through the calculation of the fundamental preliminary performance parameters of the EAP solid booster, used in the main stage of the Ariane 5 ECA. The subject that will be treated are by order:

- CEA performance and combustion analysis;
- Grain configuration analysis;
- Performance analysis;
- Nozzle dimensioning;

2.2.1 Index of symbols and constant values

This section contains a list of symbols representing variables (Table 2.1) and constant (Table 2.2) values that will be used in the following calculations.

Symbol	Meaning	Unit
\dot{m}_p	Propellant flow rate	[kg/s]
M	Mass	[kg]
ρ_{prop}	Propellant gases density	[kg/m ³]
ρ_{gas}	Exhaustion gases density	[kg/m ³]
t_b	Burning time	[s]
u_e	Outflow velocity	[m/s]
γ	Specific heat's ratio	[γ]
T_{CC}	Combustion chamber temperature	[K]
P	Pressure	[Pa]
R	Gas constant	[J/kgK]
g	Gravity acceleration	[m/s ²]
T	Thrust	[N]

Continued on next page



I_s	Specific impulse	[s]
I_{tot}	Total impulse	[Ns]
I_{vol}	Volumetric specific impulse	[kgs/m^3]
c^*	Characteristic speed	[m/s]
c_T	Thrust coefficient	[$-$]
V	Volume	[m^3]
A	Area	[m^2]
D	Diameter	[m]
r	Radius	[m]
L	Length	[m]
th	Thickness	[m]
α	Inclination angle	[rad]
ε	Nozzle ratio	[$-$]
a	Sound speed	[m/s]
Ma	Mach number	[$-$]
λ	2D loss coefficient	[$-$]

Table 2.1: Table of Variables

Symbol	Meaning	Value	Unit
ρ_{prop}	Fuel density	1690	[kg/m^3]
γ	Combustion products specific heats ratio	1.17	[$-$]
M_{dry}	Dry Mass	37	[ton]
M_{prop}	Propellant Mass	238	[ton]
H_{max}	Total Height	31	[m]
D_{max}	Diameter	3	[m]
th_{case}	Case Thickness	8	[mm]
P_{cc}	Combustion chamber maximum pressure	64	[bar]
\dot{r}_b	Radial rate of combustion	7.4	[mm/s]
I_s	Specific Impulse	275	[s]
T_{max}	Maximum thrust	6470	[kN]
\dot{m}_{out}	Gases average flow rate	2	[ton/s]
t_b	Burning time	135	[s]

Table 2.2: Table of constant and operational values [10]

2.2.2 CEA analysis

To better evaluate the engine performances a simulation is carried out using the Chemical Equilibrium Application for MatLab (CEAm) (CEA for MatLab) program. This program solves the combustion problem by minimization of the Gibbs free energy and thus computes all the important parameters of the exhaust gases. The simulation is carried out with the following input parameters:

- problem is set to rocket to solve both the combustion and nozzle;



- equilibrium is used as the CEA program tends to have problem with aluminum infused propellants and does not converge when solid particles are present;
- the booster combustion chamber pressure is unknown, thus the analysis are computed for an array of pressure from a maximum of 60 to a minimum of 40;
- for nozzle definition the outflow pressure is once again unknown and an array of values is used;
- NH₄ClO₄ (I) needs no further specification as it is present in the CEA database;
- HTPB is not present in the CEA database, thus all the needed characteristics are given as input to CEA;
- Al (cr) and Al₂O₃ (a) are used with respectively 0.89 and 0.11 mass fraction to better simulate the nano aluminum particles present in the fuel.

The data computed with the inputs above can be found in Table 2.3:

Sybol	Meaning	Value	Unit
T_c	Chamber Temperature	3785	[K]
$M_{tot}^{Mixture}$	Mixture Molar Mass	26.87	[g/mol]
γ	Specific Heat Ratio	1.3091	[$^{-}$]
M_e	Efflux Mach Number	2.9336	[$^{-}$]
a_e	Efflux Sound Speed	934.69	[m/s]
c^*	Characteristic Velocity	1730	[m/s]
I_s^{OE}	Optimum Expansion Specific Impulse	279	[s]

Table 2.3: CEA output

2.2.3 Data Analysis

To proceed with the dimensioning we used a theoretical approach thanks to the notions learned over the course.

Firstly, we used the Chemical Equilibrium Application for MatLab (CEAm) program to compute many important combustion parameters. Then, we studied three different grain configurations and their relative performances in order to choose the one that best suits our scenario.

Lastly, we conducted the nozzle analysis and dimensioning for the chosen grain configuration.

In this section, Chemical Equilibrium Application for MatLab (CEAm) data will be examined to best optimize the analysis: the software was set to operate with an equilibrium setup, considering different chamber pressures P_{cc} and pressure ratios P_{cc}/P_e to evaluate different relevant scenarios. Obtained data can be found in table: Table 2.4, Table 2.5 and Table 2.6.



	Chamber	Throat	Exit ($P_{cc}/P_e = 60$)	Exit ($P_{cc}/P_e = 50$)	Exit ($P_{cc}/P_e = 40$)
$P[\text{bar}]$	60	31.89	1	1.2	1.5
$I_s[\text{s}]$	-	122.77	284.64	279.61	273.16
ε	-	-	9.19	7.98	6.72

Table 2.4: CEA outputs table at 60bar Chamber Pressure

	Chamber	Throat	Exit ($P_{cc}/P_e = 60$)	Exit ($P_{cc}/P_e = 50$)	Exit ($P_{cc}/P_e = 40$)
$P[\text{bar}]$	50	26.63	0.83	1	1.25
$I_s[\text{s}]$	-	122.33	284.28	279.24	272.79
ε	-	-	9.21	8	6.74

Table 2.5: CEA outputs table at 50bar Chamber Pressure

	Chamber	Throat	Exit ($P_{cc}/P_e = 60$)	Exit ($P_{cc}/P_e = 50$)	Exit ($P_{cc}/P_e = 40$)
$P[\text{bar}]$	40	21.37	0.67	0.8	1
$I_s[\text{s}]$	-	121.78	283.82	278.78	272.33
ε	-	-	9.25	8.03	6.76

Table 2.6: CEA outputs table with 40bar Chamber Pressure

In order to choose the most suitable operative data, we considered the specific impulse to be the most restrictive parameter to respect. The system has to provide a specific impulse at least of 275 s. Out of all the possible configurations, we selected the one with a combustion chamber pressure of 60 bar, the closest to the maximum pressure given.

The best solution is the one with a pressure ratio $\frac{P_{cc}}{P_e} = 50$ (Table 2.5). We can now extract other relevant data from the CEAm software, as shown in Table 2.7.

	Chamber	Throat	Exit ($\varepsilon = 7.98$)
$P[\text{bar}]$	60	31.89	1.2
$T[K]$	3785.5	3578.3	2584.6
$\rho_{\text{gas}}[\text{kg/m}^3]$	5.054	2.880	0.158
$a[m/s]$	1155.029	1203.949	934.693
Ma	0.0000	1.0000	2.9336
$I_s[\text{s}]$	-	122.77	279.61
$I_{\text{vac}}[\text{s}]$	-	216.55	307.77
$c^*[m/s]$	1730.299	1730.299	1730.299

Table 2.7: CEA output table at 60bar Chamber Pressure

With this specific configuration, the nozzle is found to be sub expanded, which is a reasonable result considering the photos and videos of the launch: in fact, the combustion gases outflow is characteristic of an sub expanded nozzle. In this way, the exhaust pressure is always greater than the atmospheric pressure, even at sea level.



The outflow velocity can be found from the CEA software data as:

$$u_e = a_e \cdot M_e \cdot \lambda = 2695 \frac{\text{m}}{\text{s}}$$

where λ is the 2D loss coefficient and in function of the convergent and divergent nozzle's angles. These values are taken from typical values found in literature [1]:

$$a_{conv} = 45 \text{ deg} \quad a_{div} = 15 \text{ deg} \quad \rightarrow \quad \lambda = \frac{1 + \cos a_{div}}{2} = 0.9830$$

2.3 Grain configuration analysis

The following section will go over the sizing of the propellant grain. Three different configurations will be considered:

- Round port configuration, which provides a progressive mass flow through the nozzle;
- Star configuration, which allows an almost neutral burning;
- Moonburn grain configuration, which offers a regressive burning and decreasing mass flow over time.

Some parameters, like the maximum grain radius, are constants for each type of grain. The maximum radius r_{max} is 1.5 m, while the case thickness is 8 mm. The presence of a 1 mm thick liner to enhance grain adhesion was also taken into account. From these data, the maximum internal radius available for the propellant r_{ext} can be found:

$$r_{ext} = r_{max} - (th_{liner} + th_{case}) = 1.4820 \text{ m}$$

The total volume occupied by the propellant can be found from the total mass and fuel density as:

$$V_{prop} = \frac{M_{prop}}{\rho_{prop}} = 140.8284 \text{ m}^3$$

2.3.1 Hypothesis

The following investigation is carried out with some simplifying hypothesis, such as:

- constant burning rate $\dot{r}_b = 7.4 \text{ mm/s}$
- constant climb rate: to compute the real time-dependent thrust of the engine the atmospheric pressure is needed at each time, a steady climb rate was supposed to find the atmospheric pressure over time (using MATLAB's *atmosisa* function);
- constant combustion chamber pressure P_{cc} (as implied by the constant regression rate): this also means that the exit pressure P_e is time invariant, it is indeed:

$$P_e = \frac{P_{cc}}{P_{ratio}} = \frac{60}{50} = 1.2 \text{ bar}$$



2.3.2 Round port grain

The round port grain is maybe the most obvious choice, but it is a simple alternative to other more complex grain geometries and provides an excellent base line to compare against other configurations. For these reasons this type of grain is taken into account.

2.3.2.1 Geometry

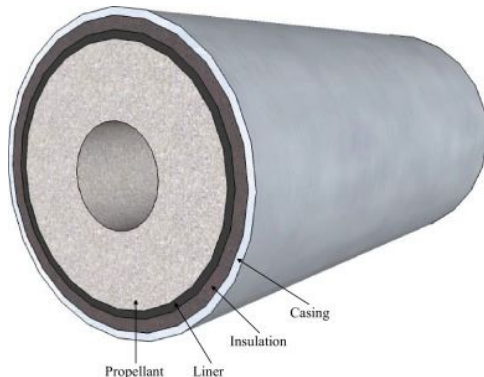


Figure 2.3: Schematic of a round port grain geometry

Given the burning time and the radial rate of combustion, the port radius is computed:

$$r_p = r_{ext} - \dot{r}_b t_b = 0.4830 \text{ m}$$

Thus the length of the propellant is:

$$l = \frac{V_p}{\pi(r_{ext}^2 - r_p^2)} = 22.8356 \text{ m}$$

With the defined parameter a CAD model of the proposed grain is realized and a technical drawing is presented:

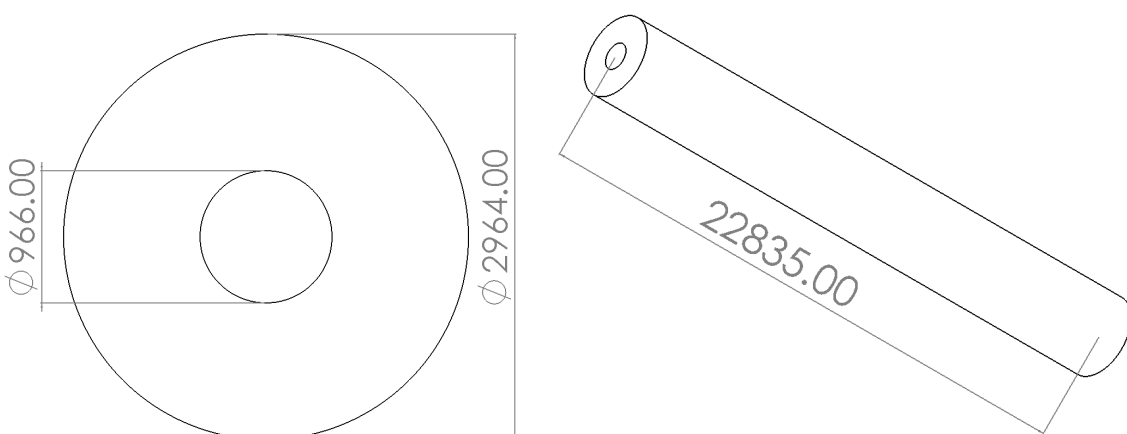


Figure 2.4: Round port grain, units in mm



2.3.2.2 Performance

In this configuration, the burning area increases over time, leading to a progressive mass flow rate (figure 2.5):

$$\dot{m}_p(t) = A_b(t) \cdot \dot{r}_b \cdot \rho_{prop} = 2\pi r(t) l \cdot \dot{r}_b \cdot \rho_{prop}$$

where $r(t)$ is the port radius that increases linearly over time.

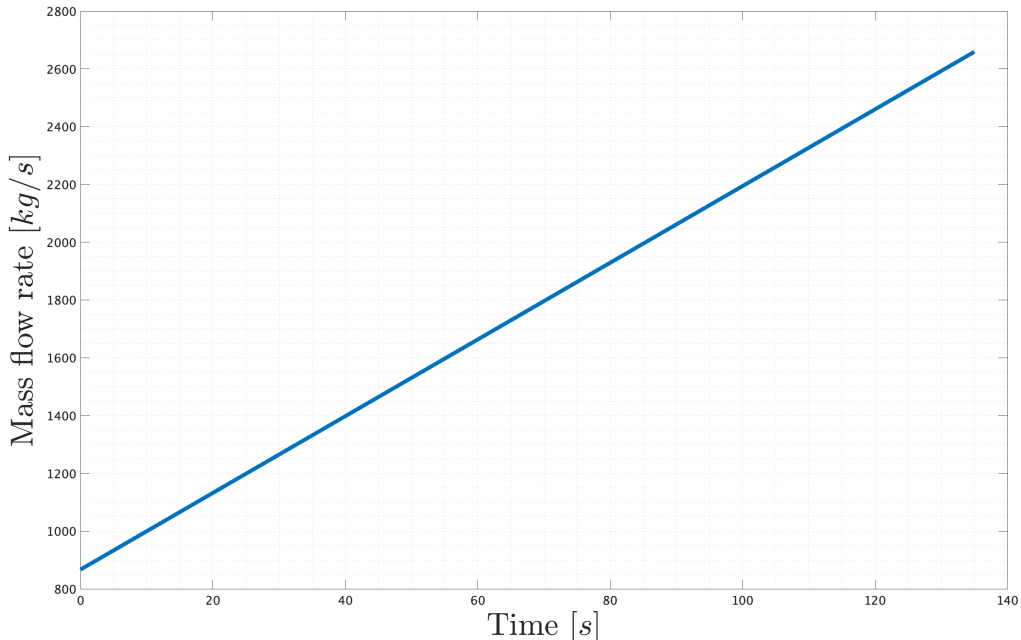


Figure 2.5: Propellant mass flow rate

The throat area must be able to handle the maximum mass flow rate present during combustion, thus:

$$A_t = c^* \cdot \frac{\max(\dot{m}_p(t))}{P_{cc}} = 0.7669 \text{ m}^2 \quad (2.1)$$

The thrust is then computed with:

$$T(t) = \dot{m} \cdot I_s \cdot g_0 + (P_e - P_{atm}(t)) \cdot A_t \cdot \varepsilon$$

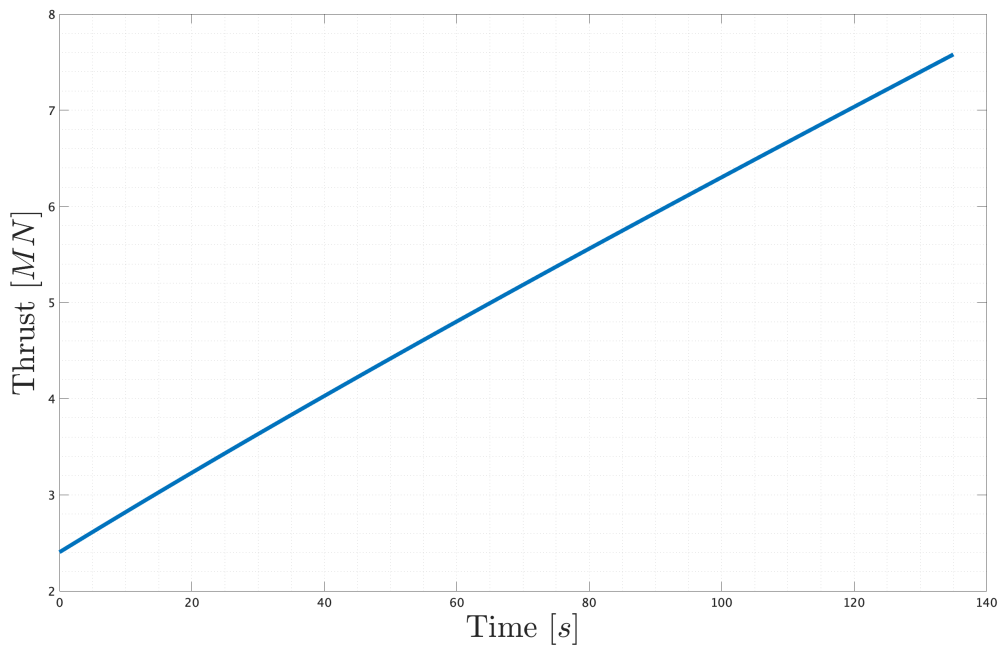


Figure 2.6: Thrust over time

2.3.3 Star Grain



Figure 2.7: EAP nozzle (left) and internal casting (right)

It is important to optimize the grain design, as it allows the rocket to reach higher performances. The star configuration has some remarkable advantages over other grain geometries: it can have a higher exposure area and a close to neutral burning, which allows the thrust to remain approximately constant during the mission.

2.3.3.1 Geometry

To begin a mean burning area is defines as:

$$A_{b,m} = 2\pi r_{p,m} \cdot l$$

where $r_{p,av}$ is the mean port radius of the round port grain, and l is the length of the round port grain.



Then, the number of tips of the star grain is defined based on values usually found in the literature, just like the height percentage. This value represents the ratio between the star tip height and the port radius $\frac{h_{tip}}{r_p}$:

$$n_{tip} = 7 \quad h\% = 0.5$$

The next step is to impose a constant burning area A_b , to do this the initial and final burning area are set to be equal:

$$A_{b,i} = A_{b,f} \rightarrow 2 n_{tip} l_{tip} \cdot l = 2\pi r_{ext} \cdot l \quad (2.2)$$

where l is the star grain length (still unknown) and l_{tip} is the tip's side length:

$$l_{tip} = \sqrt{\left(\frac{w_t}{2}\right)^2 + d_t^2}$$

where w_t is the tip's width and d_t is the tip's partial height (figure 2.8), found as:

$$w_t = 2r_p \cdot \sin \frac{\theta}{2} \quad \text{and} \quad d_t = r_p \cdot (h\% - c_t) = r_p \cdot \left(h\% - \left(1 - \cos \frac{\theta}{2}\right)\right)$$

where $\theta = \frac{2\pi}{n_{tip}}$ is the angle of the circular sector of each tip. So 2.2 is a function of the port radius r_p only, which is then easily found to be:

$$r_p = 1.1258 \text{ m} \rightarrow h_{tip} = r_p \cdot h\% = 0.5629 \text{ m}$$

Then the grain length is just a matter of:

$$l = \frac{A_{b,m}}{2\pi r_{ext}} = \frac{A_{b,m}}{2n_{tip} l_{tip}} = 15.1390 \text{ m}$$

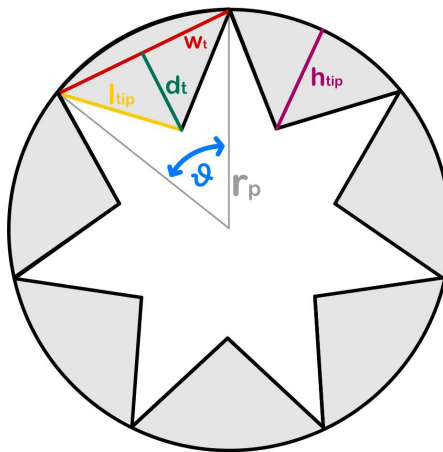


Figure 2.8: Star Geometry reference figure

With the defined parameter a CAD model of the proposed grain is realized and a technical drawing is presented:

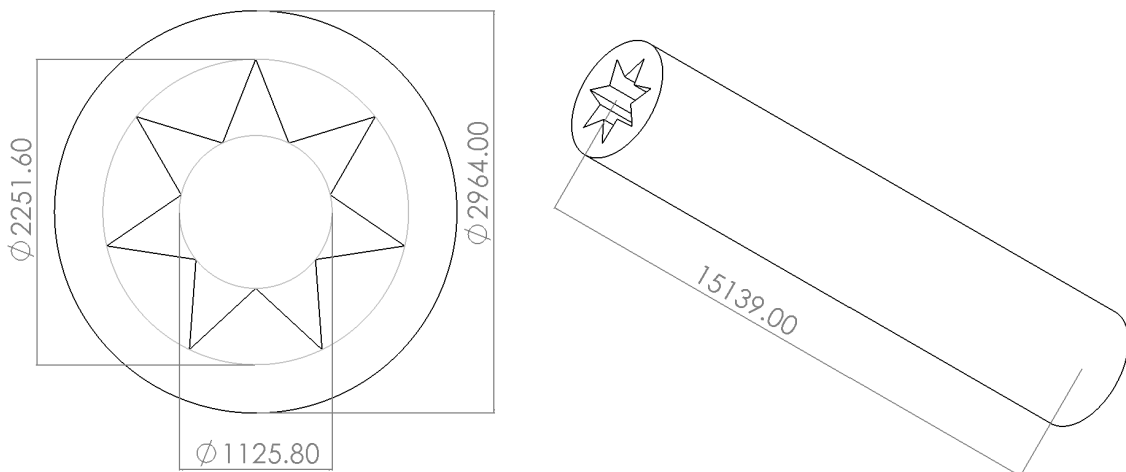


Figure 2.9: Star grain, units in mm

2.3.3.2 Performance

The mass flow rate is supposed to be constant since both the burning area and regression rate follow the same assumption:

$$\dot{m}_p = \rho_{prop} \cdot \dot{r}_b \cdot A_{b,m} = 1763.0 \text{ kg}$$

The throat area is as in 2.1:

$$A_t = c^* \cdot \frac{\dot{m}_p}{P_{cc}} = 0.5084 \text{ m}^2$$

As before, the atmospheric pressure is computed by supposing a constant climb rate and the standard model for the atmosphere. The thrust is then:

$$T(t) = \dot{m}_p \cdot v_e + (P_e - P_{atm}(t)) \cdot A_t \varepsilon$$

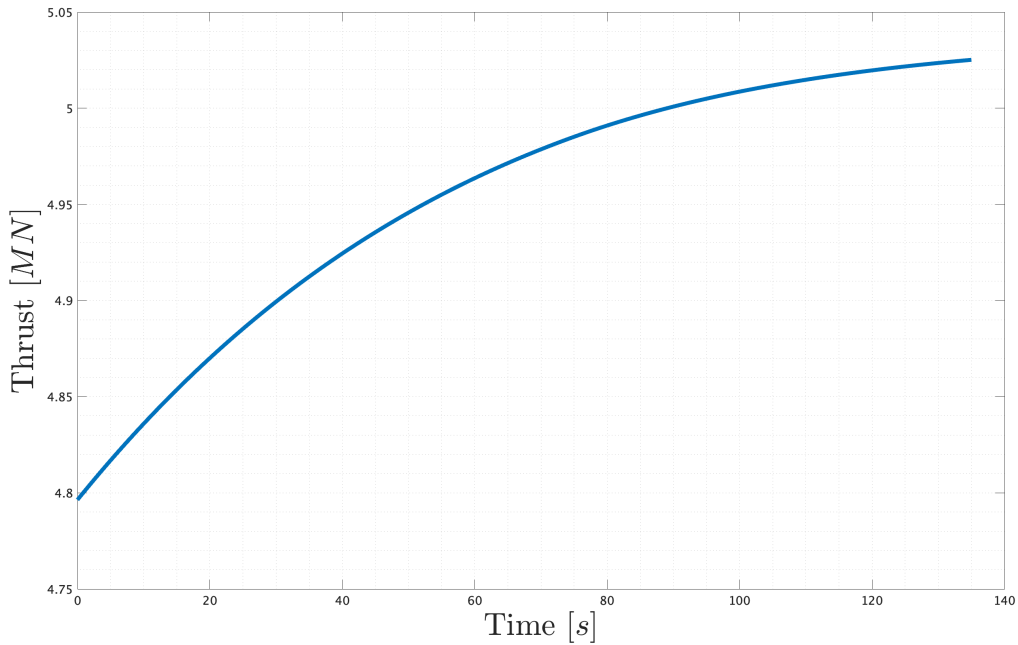


Figure 2.10: Thrust over time

2.3.4 Moonburn

It is also possible to have regressing grain configuration, meaning that the burning area, and thus the mass flux and thrust, decreases over time.

One commonly used geometry is the *moonburn* one (figure 2.11), a geometry with a circular inner port de-centered with respect to the booster.

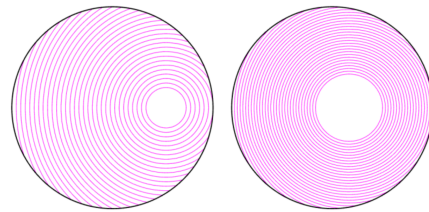


Figure 2.11: Moonburn grain geometry

2.3.4.1 Geometry

In order to maintain the same total impulse as previous configurations the initial port radius is set equal to the one used in the round port configuration:

$$r_p^{moonburn} = r_p^{round} = 0.4830 \text{ m}$$

And to maintain the same propellant volume also the same grain length is used:

$$l^{moonburn} = l^{round} = 22.8356 \text{ m}$$



The most important parameter left to find is the distance of the port's radius from the booster's center r_c . The possible values are:

$$0 < r_c < (r_{ext} - r_p) = 0.9990 \text{ m}$$

Different values of r_c are evaluated and the burn area A_b is plotted over time:

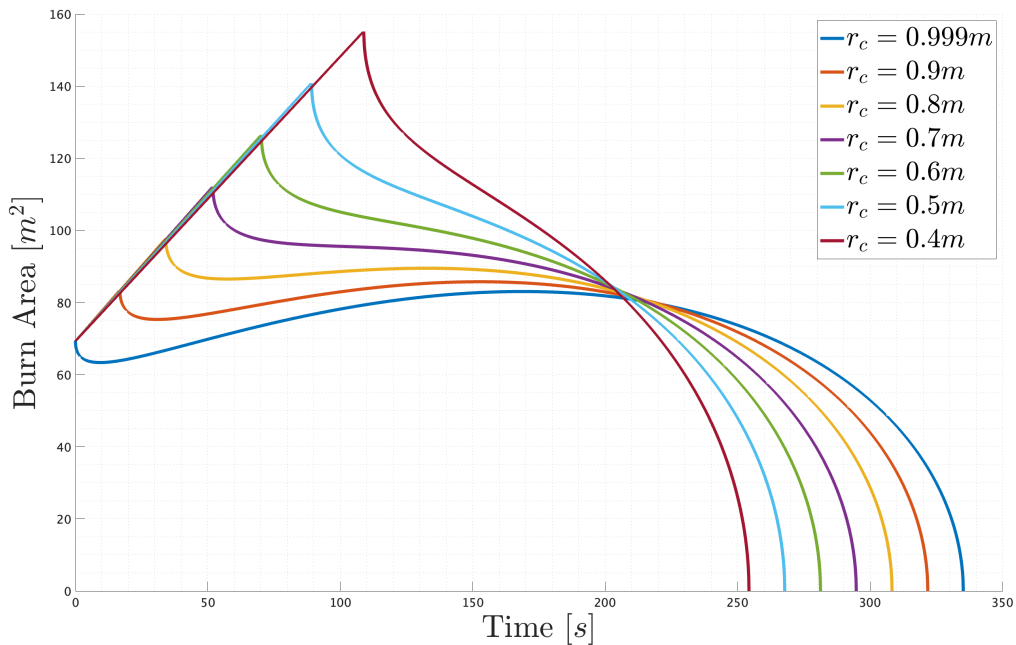


Figure 2.12: Burn Area for different values of r_c

As expected a lower value of r_c leads to a longer fraction of the burning area being linear, just like the round port grain; as soon as the combustion reaches the outer edge of the booster case the burning area changes trend and begins descending.

Also, the combustion time t_b is heavily dependent on the position of the port. With a port further away from the booster's centre the combustion will take longer to burn all the propellant.

With the defined parameter a CAD model of the proposed grain is realized and a technical drawing is presented:

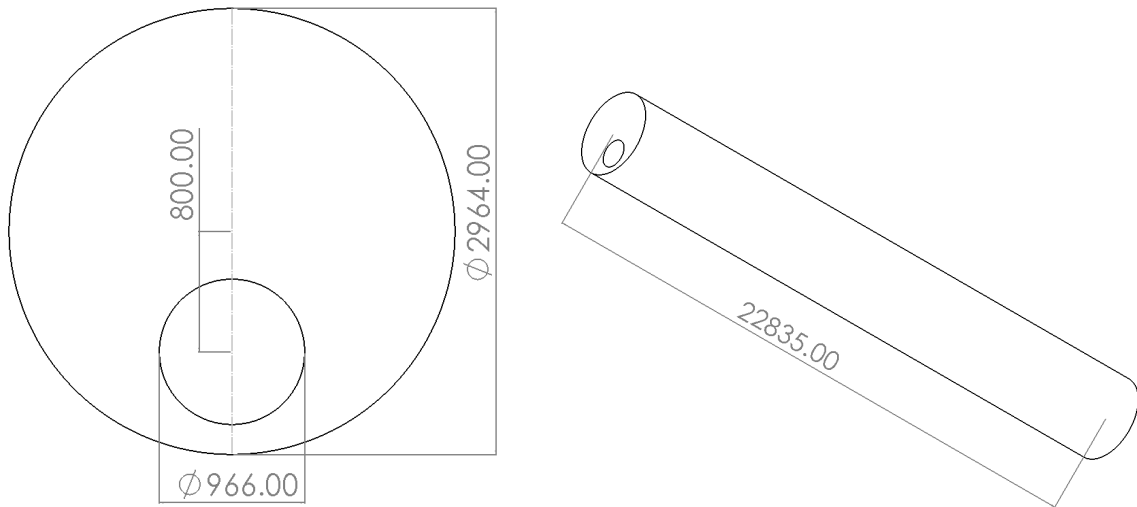


Figure 2.13: Moonburn grain, units in mm

2.3.4.2 Performance

The value $r_c = 0.8$ m is selected as it provides an initial spike in the mass flow rate (that helps to ensure a high initial velocity and thus stability) and still provides a kind-of regressive burn area. To compute the evolution of A_b first the enlarging port is intersected with the booster's case and then the available burn area is found:

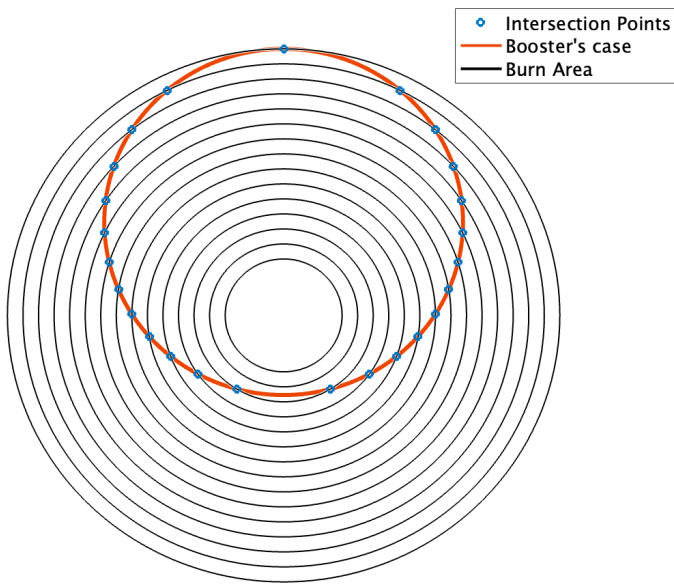


Figure 2.14: Burn Area over time

This area $A_b(t)$ is then used to find the propellant mass flow rate:

$$\dot{m}_p(t) = A_b(t) \cdot \dot{r}_b \cdot \rho_p$$

which has the same trend as the yellow plot in figure 2.12.



The throat area, as before, is found via:

$$A_t = c^* \cdot \frac{\max(\dot{m}_p)}{P_{cc}} = 0.3228 \text{ m}^2$$

Thus the thrust is:

$$T(t) = \dot{m}_p(t) \cdot u_e + (P_e - P_{atm}(t)) \cdot A_t \varepsilon$$

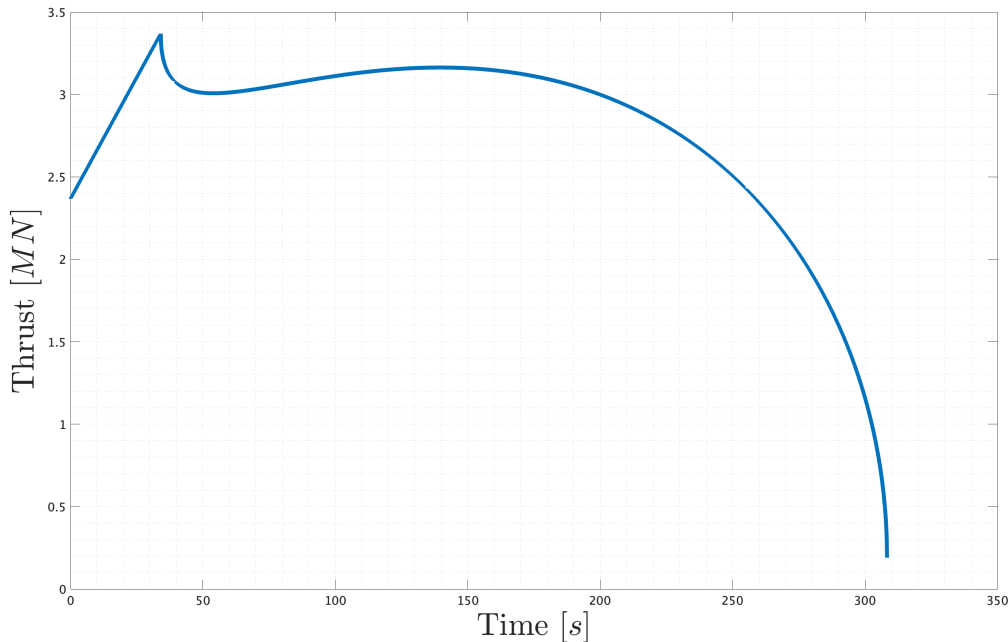


Figure 2.15: Thrust over time

2.3.5 Conclusion

Looking at the results, the only configuration that allows reaching the maximum thrust of 6470 kN , as indicated in the literature [10], is the single-port configuration. Therefore, a round-port configuration is assumed to carry out the following calculations.

2.4 Performance - other parameters

Now the grain configuration has been selected, other important performance parameters can be evaluated.

2.4.1 Coefficient of thrust and characteristic velocity

The coefficient of thrust is defined as:

$$c_T(t) = \frac{T(t)}{P_{cc}(t) \cdot A_t} \quad c_T^{\text{@OE}} = 1.5847$$



Since the combustion chamber pressure is assumed constant this parameter loses part of its significance as with this hypothesis there is no direct correlation between T and P_{cc} ; nonetheless it can be computed and it can provide some insights.

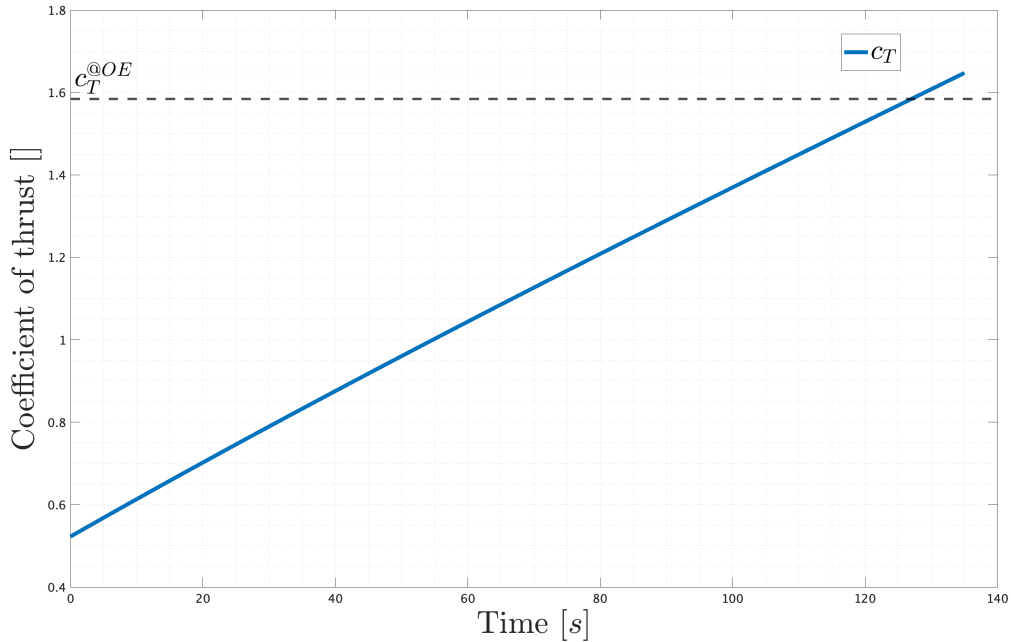


Figure 2.16: Coefficient of thrust over time

The value at optimal expansion is near the maximum: this is expected as the maximum thrust for a given chamber pressure is obtained when all the available ΔP is used to accelerate the flux, and not to provide static thrust.

Something similar as per the coefficient of thrust could be said for the characteristic velocity, in this case only the value provided by the CEA simulation is reported and can be found in table 2.7.

2.4.2 Specific impulse

The specific impulse quantifies how effectively the engine utilizes its propellant to generate thrust. It is defined as:

$$I_s(t) = \frac{T(t)}{\dot{m}_p \cdot g_0} \quad I_s^{@OE} = 279.6 \text{ s}$$

and thus it follows the thrust's trend:

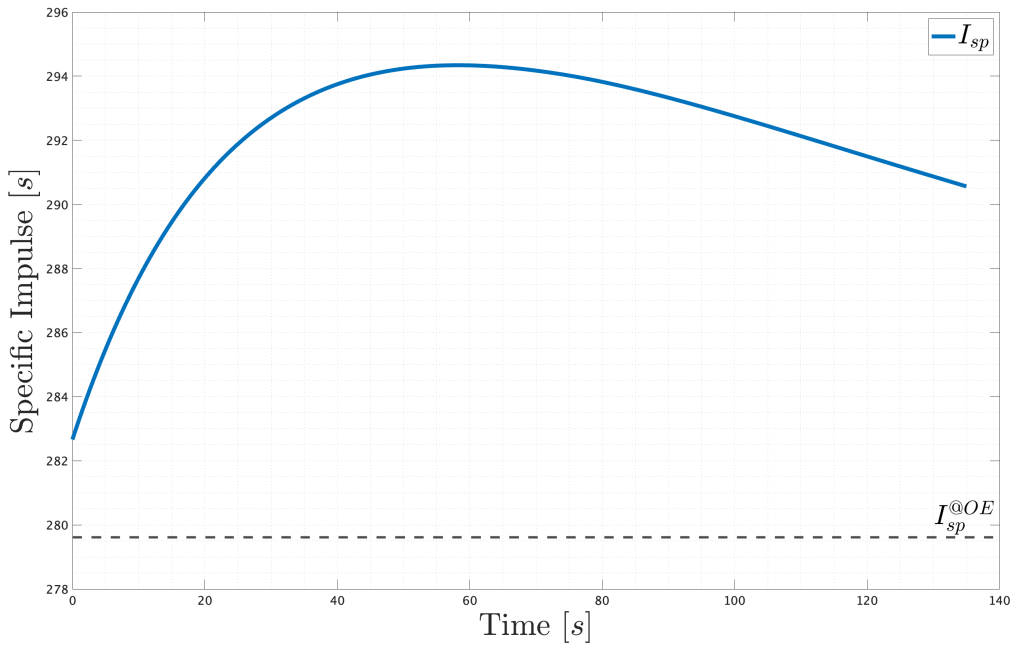


Figure 2.17: Specific impulse over time

It is evident that the $I_s(t)$ is always above its value at optimal expansion since as per design the engine is always sub-expanded.

2.4.3 Total and volumetric impulse

The total impulse is defined as:

$$I_{tot} = \int_0^{t_b} T(t)dt = 6.82 \text{ MN s}$$

while the volumetric:

$$I_{vol}(t) = I_s(t) \cdot \rho_{prop} \quad I_{vol}^{\text{@OE}} = I_s^{\text{@EO}} \cdot \rho_{prop} = 4.72 \cdot 10^5 \frac{\text{s kg}}{\text{m}^3}$$

2.5 Nozzle Dimensioning

The nozzle is assumed to have a conical trunk shape. The convergent and divergent angles can be respectively fixed at 45 deg and 15 deg, having considered typical values from the literature [1]. The maximum diameter D_{max} is assumed to be 3m from the initial known data.

For the following dimensioning, we considered the maximum mass flow with a single-port grain configuration obtained from the previous grain analysis, which is

$$\dot{m}_p(t) = 2659.2 \frac{\text{kg}}{\text{s}}$$

Therefore, the throat area and diameter can be calculated as:



$$A_t = \frac{c^* \dot{m}_p(t)}{P_{cc}} = 0.7669 \text{ m}^2 \quad D_t = \sqrt{\frac{4A_t}{\pi}} = 0.9881 \text{ m}$$

The discharge area and diameter can be calculated knowing the expansion ratio $\varepsilon = 7.98$:

$$A_e = \varepsilon A_t = 6.1196 \text{ m}^2 \quad D_e = \sqrt{\frac{4A_c}{\pi}} = 2.7914 \text{ m}$$

Knowing the inclinations, we can find the length of both the divergent and convergent:

$$L_{div} = \frac{D_e - D_t}{2 \tan \alpha_{div}} = 3.3649 \text{ m} \quad L_{conv} = \frac{D_{max} - D_t}{2 \tan \alpha_{conv}} = 1.0059$$

$$L_{tot} = L_{div} + L_{conv} = 4.3708 \text{ m}$$

Due to the divergence of the nozzle some of the flow doesn't give any contribution to the thrust production because of the velocity radial component. This effect can be summarized in a loss coefficient λ which can be found as:

$$\lambda = \frac{1 + \cos \alpha_{div}}{2} = 0.9830$$



3 EPC: Etage Principal Cryotechnique

Ariane 5's cryogenic H173 main stage called the Etage Principal Cryotechnique (EPC). It consists of a 5.4 m (18 ft) diameter by 30.5 m (100 ft) high tank with two compartments, one for liquid oxygen and one for liquid hydrogen, and a Vulcain 2 engine at the base with a vacuum thrust of 1390 kN.



Figure 3.1: Ariane 5 Stages Breakdown [4]

In order to hold the extra liquid oxygen needed for the EPC core stage, the capacity of the liquid oxygen tank was increased by 16 t, compared to the previous iterations of the Ariane 5. This change was obtained by relocating the common tank bulkhead between the liquid



oxygen tank and the liquid hydrogen tank and reinforcing the structure element, increasing the allowable propellant mass to 150 t of LOX and 25 t of LH₂.

The EPC stage operates for nearly 540 s. It also provides roll control during the main propulsion phase. At shut down, EPC separates from the upper composite at an altitude between 160 km and 210 km, depending on the mission's trajectory, and performs a destructive re-entry in the atmosphere over the Atlantic Ocean.

3.1 Characterization of the Stage

The following section will provide an introduction to the elements the elements that characterize the EPC. Therefore the subject below will be described:

- Propellant
- Engine
- Operational data and characteristics of the engine



Figure 3.2: Ariane 5 EPC and Vulcain 2 engine previous to integration [4]



3.1.1 Characterization of the propellant

3.1.1.1 Liquid Oxygen

Liquid oxygen (LOX) is a desirable and widely used oxidizer in large rocket engines, thanks to its relatively high performances. LOX is a noncorrosive and nontoxic liquid that will not cause the deterioration of clean container walls. Because LOX evaporates rapidly at ambient conditions, it cannot be stored readily for any extended length of time. When LOX is used in large quantities, it is often produced very close to its geographical point of application. It is necessary to insulate all lines, tanks, valves, and parts that contain liquid oxygen in order to reduce evaporation losses and heat absorption. External drainage provisions have to be made on all LOX tanks and lines to allow the water that condenses on the cold outside walls to drain from the rocket during launch preparations.

Propellant	LOX	LH2
Chemical formula	O_2	<i>para</i> – H_2
Molecular mass	31.988	2.016
Melting or freezing point [K]	54.8	14.0
Boiling point [K]	90.2	20.27
Heat of vaporisation [kJ/kg]	213	446
Specific heat [kcal/kgK]	0.4 (65K)	2.34 (20.27K)
Density	1.14 (90.4 K) 1.23 (77.6 K) 0.87 (53.7 K) 0.19 (90.4 K)	0.071 (20.27 K) 0.076 (14 K) 0.024 (14.3 K) 0.013 (20.4 K)
Viscosity (centipoises)		
Vapor pressure (MPa)	0.0052 (88.7 K)	0.2026 (23 K) 0.87 (30 K)

Table 3.1: Propellant properties tables [1]

3.1.1.2 Liquid Hydrogen

Oxidizer	Fuel	Mixture Ratio		Average Specific Gravity	Chamber Temp.(K)	Chamber c^* (m/sec)	\bar{M} , (kg/mol)	I_s (sec)		
		By Mass	By Volume					Shifting	Frozen	k
Oxygen	Methane	3.20	1.19	0.81	3526	1835	20.3		296	1.20
		3.00	1.11	0.80	3526	1853			311	
	Hydrazine	0.74	0.66	1.06	3285	1871	18.3		301	1.25
		0.90	0.80	1.07	3404	1892	19.3	313		
Hydrogen		3.40	0.21	0.26	2959	2428	8.9		386	1.26
		4.02	0.25	0.28	2999	2432	10.0	389.5		

Table 3.2: Theoretical Chamber Performance of Liquid Rocket Propellant Combinations [1]



As shown in Table 3.2, when burned with oxygen hydrogen gives a high performance colorless flame. Of all known fuels, liquid hydrogen is by far the lightest and the coldest, having a density of 0.07 and a boiling point of about 20 K. This extremely low fuel density requires bulky and large fuel tanks, which necessitate rather large vehicle volumes. The extremely low storage temperatures limit the available materials for pumps, cooling jackets, tanks, and piping because many metals become brittle at such temperatures. Because of their very low temperatures, liquid hydrogen tanks and supply lines have to be well insulated to minimize hydrogen evaporation or the condensation of moisture or air on the outside. A vacuum jacket has often been used in addition to the insulating materials.

LOX and LH₂ are on-hypergolic propellants, therefore they require an ignition source to burn. Liquid hydrogen is used with liquid oxygen in the Ariane V and it's one of the best combination in terms of specific impulse (payload capability usually increases greatly for relatively small increases in specific impulse) and average density (as shown in Table 3.2).

The tanks are only few millimetres thick: 1.3 mm for the hydrogen and 4.7 mm for the oxygen. Given the structural characteristics of the main stage, when the tanks are empty they have to be pressurised to prevent them buckling under their own weight.

3.1.2 Engine description: Vulcan 2 Engine

The Vulcain 2 engine is designed by Snecma Moteurs for Ariane 5 ECA and is an upgraded version the Vulcain 1 engine.

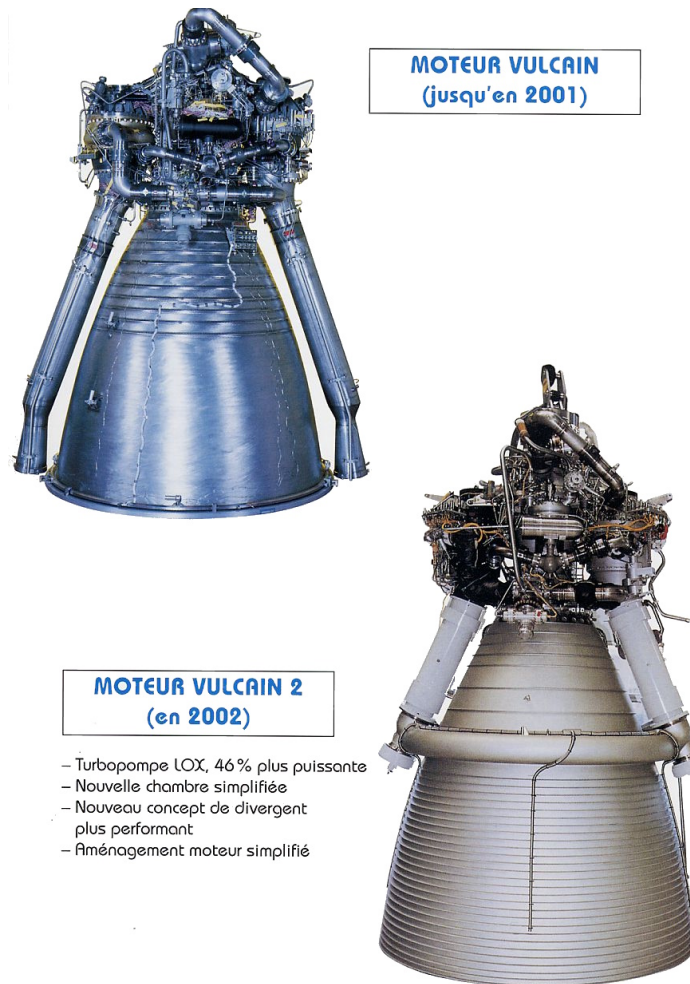


Figure 3.3: Comparison between Vulcan 1 (top left) and Vulcan 2 (bottom right)

The rocket engine works through a gas-generator cycle and provides 8 % of Ariane's thrust at liftoff. The rest of the thrust is provided by the two EAPs. Thanks to the Vulcain 2 it was possible to increase the payload capacity of Ariane 5 to 6.8 t/m and increase the engine's specific impulse by 3 s over the basic model.

These achievements were possible thanks to a complete redesign based on the proven technology of its predecessor. Here are listed some of the features that were included in this iteration of the engine:

- It operates under slightly higher pressure with a mixture ratio that has 20 % more liquid oxygen than the Vulcain 1. Because of this change in the mixture, a new oxygen turbopump was developed.
- Higher flow rate is achieved via a 16 % hydrogen inlet pressure increase, driving the pump at 35 680 rotations per minute. The gain in the hydrogen turbine inlet pressure, in turn, is produced through a 22 % increase in the hot gas flow coming from the gas generator, which at the same time satisfies the 30 % increase needed for the oxygen turbine.
- *Oxidizer : Fuel* ratio is increased to 6.3 and the expansion ratio by 30 %.



- Turbine exhaust gas are injected into the main flow.
- The H₂ used for the cooling of the upper part is then injected into the nozzle at a specific expansion ratio and used as a film for the downstream part of the nozzle section.

3.1.3 Operational data

The Vulcain engine operates for just under 10 minutes before it shutdowns. At this point, at an attitude of around 145 km, the main stage separates and follows a side ballistic trajectory during which it is spun on a transversal axis before re-entering the atmosphere. Most of it burns up into the atmosphere and the remaining parts fall into the Pacific Ocean, about 2000 km off the coast of South America.

ENGINE	SNECMA MOTEURS VULCAIN 2
Length	3,60 m
Diameter	2,15 m
Dry weight	1935 kg
Propellant	Liquid Oxygen (LOX) and Liquid Hydrogen (LH ₂)
Mixture ratio	6.1
Power of the turbopump	3,7 – 6,6 MW (LOX) / 9,9 – 20,4 MW (LH ₂)
Thrust, vacuum	1350 kN
Thrust, sea level	960 kN
Specific impulse, vacuum	433 s
Specific impulse, sea level	320s
Section ratio	58.5
Burn time	540 s

Table 3.3: SNECMA Vulcan Engine specifications table [6]

Propellants	LOX	LH ₂
Propellant mass and flow rate at combustion chamber inlet [kg/s]	44.9	257.1
Combustion chamber inlet pressure [MPa]	18.45	15.6
Combustion chamber inlet temperature [C]	-237	-176.5
Combustion chamber pressure [MPa]		11.5
Combustion chamber temperature [C]		3250

Table 3.4: Temperature and pressure parameters for the Vulcan engine

3.2 Modelling of the engine

The current section goes through the calculation of the fundamental preliminary performance parameters of the Vulcain 2 engine, used in the main stage of the Ariane 5 ECA. The subject that will be treated are by order:

- CEA performance and combustion analysis;



- Dimensioning of the nozzle;
- Analysis of the coefficient of Thrust and Specific impulse;
- Combustion chamber and injection plate;
- Pressurization system;
- Turbopump system;
- Cooling system.

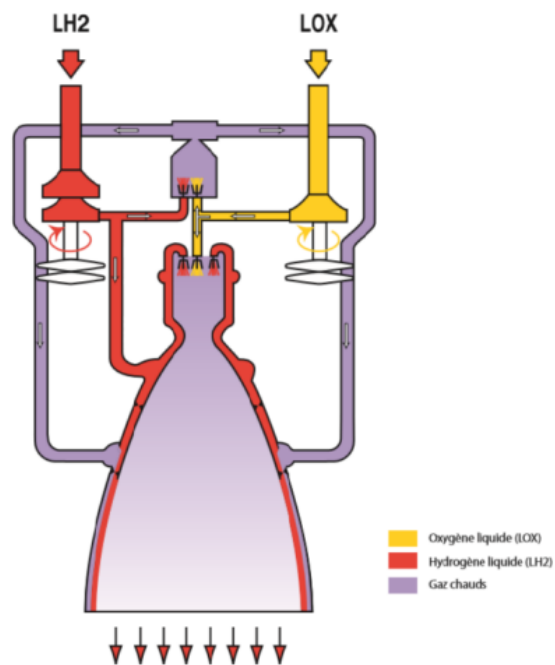


Figure 3.4: Operating principle of the Vulcain 2 engine [5]

3.2.1 Index of variable and constants

This section contains a list of symbols representing variables (Table 3.5) and constant (Table 3.6) values that can be found in the following calculations.

Symbol	Meaning	Unit
\dot{m}_{ox}	Oxidizer flow rate	[kg/s]
\dot{m}_f	Fuel flow rate	[kg/s]
m_{ox}	Mass of Oxidizer	[kg]
m_f	Mass of Fuel	[kg]
ρ_{ox}	Oxidizer density	[kg/m ³]
ρ_f	Fuel density	[kg/m ³]
ρ_{av}	Average density	[kg/m ³]
V_{ox}	Oxidizer volume	[m ³]

Continued on next page



V_f	Fuel volume	[m^3]
t_b	Time of burning	[s]
v_e	Outflow velocity	[m/s]
M_{mol}	Molar mass	[$kg/kmol$]
γ	Specific heat ratio	[$-$]
T	Temperature	[K]
P	Pressure	[Pa]
R	Universal constant of perfect gasses	[$J/mol * K$]
$R*$	Relative mass constant	[$J/kg * K$]
T	Thrust	[N]
I_{sp}	Specific impulse	[s]
$I_{sp,vol}$	Volumetric Specific impulse	[$kg * s/m^2$]
$I_{sp,tot}$	Total Specific impulse	[$N * s$]
Γ	Vandenerkerchkove function	[$-$]
c^*	Equivalent speed	[m/s]
c_T	Thrust coefficient	[$-$]
η	Losses coefficient	[$-$]
A	Area	[m^2]
D	Diameter	[m]
ε	Nozzle ratio	[$-$]
M	Mach number	[$-$]
λ	Loss factor	[$-$]
L^*	Characteristic length	[m]
c_D	Discharge coefficient	[$-$]
N	Number of injections	[$-$]
u	Velocity	[m/s]
z	Altitude	[m]
a	Temperature variation rate with altitude	[K/m]

Table 3.5: Table of Variables



Symbol	Meaning	Value	Unit
t_b	Time of burning	540	[s]
P_c	Chamber pressure	11.5	[MPa]
\dot{m}_p	Propellant mass flow	320	[kg/s]
ε	Nozzle ratio	58.5	[-]
OF	Mixture ratio	6.1	[-]
ρ_f	Fuel density	71	[kg/m ³]
ρ_{ox}	Oxidizer density	1140	[kg/m ³]
a	Temperature variation with altitude	0.0065	[K/m]
P_{std}	Standard Pressure (at sea level)	101325	[Pa]
T_{std}	Standard Temperature (at sea level)	288.15	[K]
g_0	Gravity constant	9.81	[m/s ²]
R	Universal constant of perfect gasses	8.3145	[J/K * mol]
R^*	Specific gas constant for air	287.2	[J/Kg * K]

Table 3.6: Table of constants and operational values [6]

3.2.2 Hypothesis for the calculations

In the following sections, several hypotheses will be used to simplify the calculations, nonetheless maintaining a certain degree of accuracy:

- One-dimensional flow;
- Isentropic flow;
- Adiabatic flow;
- Stationary flow;
- Equilibrium conditions from inlet to throat;
- Constant exhaust pressure;

3.2.3 CEA analysis

To better evaluate the engine performances a simulation is carried out using the Chemical Equilibrium Application for MatLab (CEAm) program. This program solves the combustion problem by minimization of the Gibbs free energy and thus computes all the important parameters of the combustion gases. The simulation is carried out with this input parameters:

- problem is set to rocket to solve both the combustion and nozzle;
- frozen is set to nfz with station 1 to make the flow frozen at the throat;
- combustion chamber pressure is set to 115 bar;
- the OF is set to 6.1;
- for nozzle definition the expansion ratio is set to 58.5;



- fuel and ox are defined respectively as H₂(L) and O₂(L) in order to use the ones provided in the CEA library.

The data computed with the inputs above can be found in Table 3.7:

Symbol	Meaning	Value	Unit
T_c	Chamber Temperature	3990	[K]
$M_{tot}^{Mixture}$	Mixture Molar Mass	14.3079	[g/mol]
γ	Specific Heat Ratio	1.1823	[-]
M_e	Efflux Mach Number	4.5312	[-]
a_e	Efflux Sound Speed	961.68	[m/s]
a_c	Combustion Chamber Sound Speed	1653	[m/s]
c^*	Characteristic Velocity	2361	[m/s]
P_e	Efflux Pressure	$1.4139 \cdot 10^4$	[P _a]
$I_{sp,OE}$	Optimum Expansion Specific Impulse	444	[s]

Table 3.7: CEA outputs table

3.2.4 Nozzle Dimensioning

Firstly, knowing the mass flow rate of propellant and the OF ratio, the mass flow rates of both the oxidizer and the fuel are given by:

$$\dot{m}_{ox} = \frac{OF}{OF + 1} \dot{m}_p = 274.93 \frac{\text{kg}}{\text{s}} \quad \dot{m}_f = \frac{1}{OF + 1} \dot{m}_p = 45.0704 \frac{\text{kg}}{\text{s}}$$

The convergence and divergence can be hypothesized from typical values found in literature [1]:

$$\alpha_{conv} = 45 \text{ deg} \quad \alpha_{div} = 15 \text{ deg}$$

Thus the 2D loss coefficient can be computed as:

$$\lambda = \frac{1 + \cos \alpha_{div}}{2} = 0.9830$$

Using c^* , the propellant mass flow rate \dot{m}_p and combustion chamber pressure P_c the throat area is:

$$A_t = c^* \cdot \frac{\dot{m}_p}{P_c} = 0.0657 \text{ m}^2 \quad D_t = \sqrt{\frac{4A_t}{\pi}} = 0.2892 \text{ m}$$

Since that the nozzle ratio is known, the outflow area and diameter can be easily calculated:

$$A_{outflow} = \varepsilon \cdot A_{throat} = 3.8433 \text{ m}^2 \quad D_{outflow} = \sqrt{\frac{4 \cdot A_{outflow}}{\pi}} = 2.2121 \text{ m}$$



The combustion chamber is assumed to be a stagnation zone with a Mach number of $M_c = 0.2$. The sound velocity at this stage is known from CEA output, so the combustion chamber velocity can be easily found:

$$v_c = M_c \cdot a_c = 330.60 \frac{\text{m}}{\text{s}}$$

Knowing the combustion chamber pressure and the Chamber Temperature from CEA, first the combustion products density is:

$$\rho_c = \frac{P_c}{R_c \cdot T_c} = 4.9598 \frac{\text{kg}}{\text{m}^3}$$

where R_c is the specific gas constant for the combustion products.

Now the combustion chamber area and diameter are:

$$A_c = \frac{\dot{m}_p}{\rho_c \cdot v_c} = 0.1952 \text{ m}^2 \quad D_c = \sqrt{\frac{4A_c}{\pi}} = 0.4985 \text{ m}$$

With the help of the aforementioned values, the length of the converging and diverging parts of the nozzle can finally be estimated by:

$$L_{conv} = \frac{D_c - D_{throat}}{2 \tan(\alpha_{conv})} = 0.1046 \text{ m} \quad L_{div} = \frac{D_{outflow} - D_{throat}}{2 \tan(\alpha_{div})} = 3.5882 \text{ m} \quad (3.1)$$

$$L_{tot} = L_{conv} + L_{div} = 3.6928 \text{ m} \quad (3.2)$$

These dimensions were used to create a 3D model, its representation can be seen in Figure 3.5:

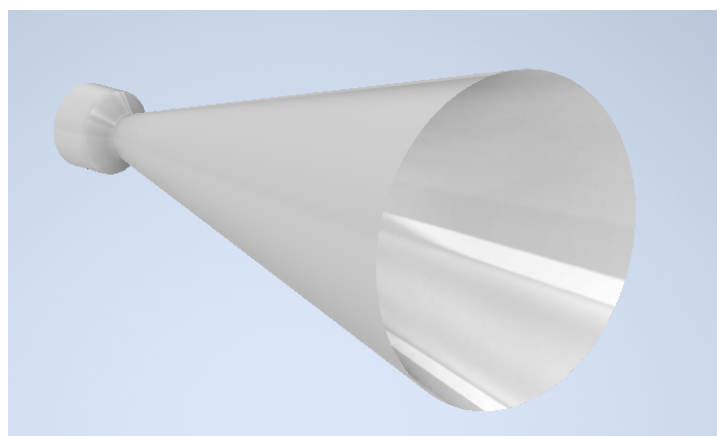


Figure 3.5: 3D model of the nozzle obtained using measurements of Equation (3.1) and Equation (3.2)

3.2.5 Performances

3.2.5.1 Thrust

To compute the real thrust over time it is necessary to know the atmospheric pressure over time. In order to do this, we used the MATLAB function *atmosisa.m*, which considers the aforementioned standard atmosphere model.

Using the data from CEA we can compute the ideal and real efflux velocity as:

$$v_{e,real} = v_e = v_{e,id} \cdot \lambda = M_e a_e \cdot \lambda = 4357.6 \cdot 0.9830 = 4283.5 \frac{\text{m}}{\text{s}}$$

Then, the thrust vector is as follows (figure 3.6):

$$T(t) = \dot{m}_p \cdot v_e + (P_e - P_{amb}(t)) \cdot A_e$$

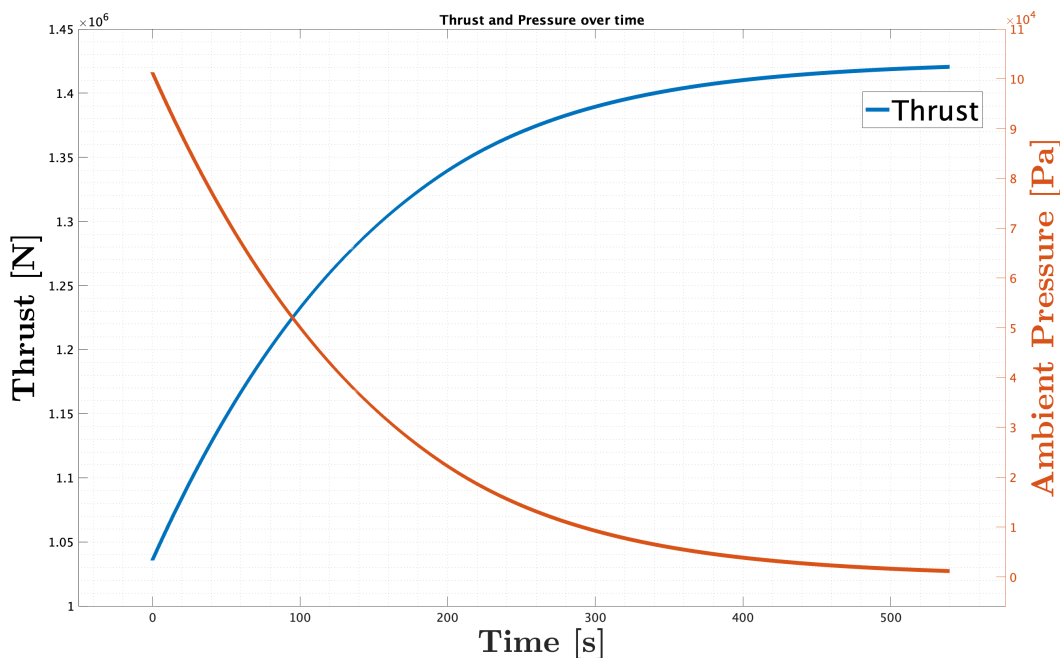


Figure 3.6

3.2.5.2 Thrust coefficient

Once the thrust over time is known, the thrust coefficient is found with:

$$c_T(t) = \frac{T(t)}{P_c \cdot A_t} \quad c_T^{@OE} = 1.8143$$



3.2.5.3 Specific Impulse

The specific impulse over time (figure 3.7) has the same trend as the thrust, since a constant mass flow rate has been hypothesized:

$$I_{sp}(t) = \frac{T(t)}{\dot{m}_p \cdot g_0} \quad I_{sp}^{\text{@OE}} = 444 \text{ s}$$

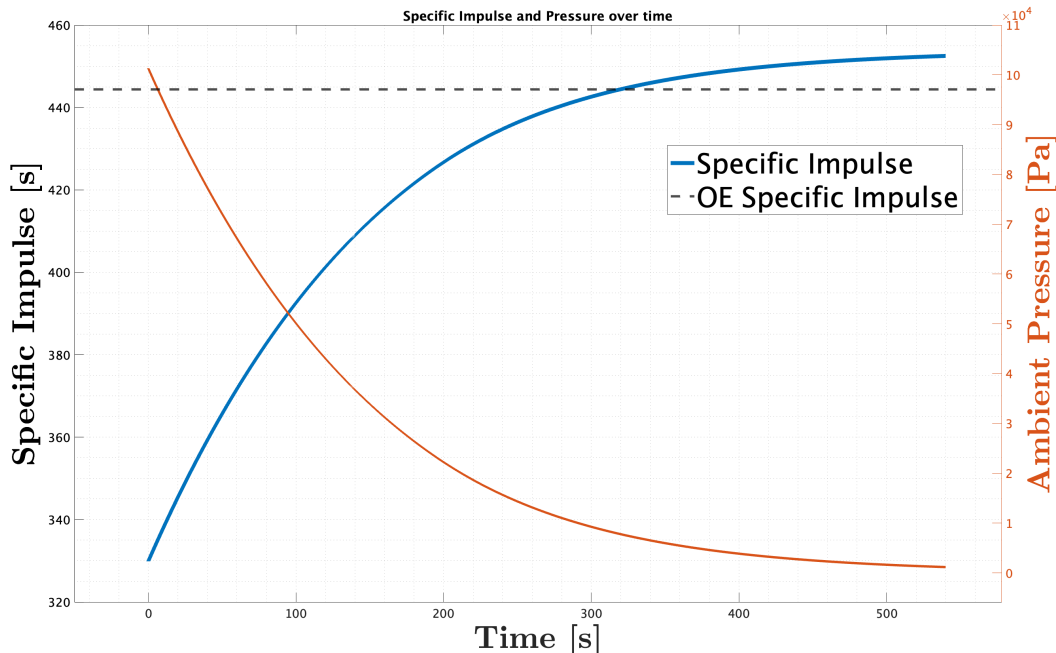


Figure 3.7

3.2.5.4 Volumetric Impulse

Knowing the burning time of the combustion, the masses of both propellants can be estimated as:

$$m_{ox} = \dot{m}_{ox} \cdot t_b = 148\,461.97 \text{ kg} \quad m_f = \dot{m}_f \cdot t_b = 24\,338.03 \text{ kg}$$

Since the fuel and oxidizer densities are known, the volumes are evaluated like:

$$V_{ox} = \frac{m_{ox}}{\rho_{ox}} = 130.23 \text{ m}^3 \quad V_f = \frac{m_f}{\rho_f} = 324.79 \text{ m}^3$$

Then, the average propellant density is computed as follows:

$$\rho_{av} = \frac{m_{ox} + m_f}{V_{ox} + V_f} = 365.31 \frac{\text{kg}}{\text{m}^3}$$

Then the volumetric impulse is found:



$$I_{sp,v}(t) = I_{sp}(t) \cdot \rho_p \quad I_{sp,v}^{\text{@OE}} = 1.62326 \cdot 10^5 \frac{\text{s kg}}{\text{m}^3}$$

Also the total impulse is:

$$I_{tot} = \int_0^{t_b} T(t) dt = 718 \text{ MN s}$$

3.2.5.5 Mach number

Even though the trend of the Mach number along the nozzle is not of major importance, it can be of interest.

The following equation is used to find the area ratio for a specific value of the Mach number:

$$\frac{A_2}{A^*} = \frac{1}{M_2} \left[\frac{2}{\gamma + 1} \left(1 + \frac{\gamma - 1}{2} M_2^2 \right) \right]^{\frac{\gamma+1}{2(\gamma-1)}} \quad (3.3)$$

Using MATLAB's *fso*ve we can find the solution to:

$$0 = \frac{1}{M_2} \left[\frac{2}{\gamma + 1} \left(1 + \frac{\gamma - 1}{2} M_2^2 \right) \right]^{\frac{\gamma+1}{2(\gamma-1)}} - \frac{A_2}{A^*} \quad (3.4)$$

where $\frac{A_2}{A^*}$ is a vector of area ratios that goes from the combustion chamber $\frac{A_c}{A_t}$ to the efflux $\frac{A_e}{A_t} = \varepsilon$.

The computed mach number can then be plotted over the longitudinal coordinate starting at the beginning of the convergent section and ending at the efflux:

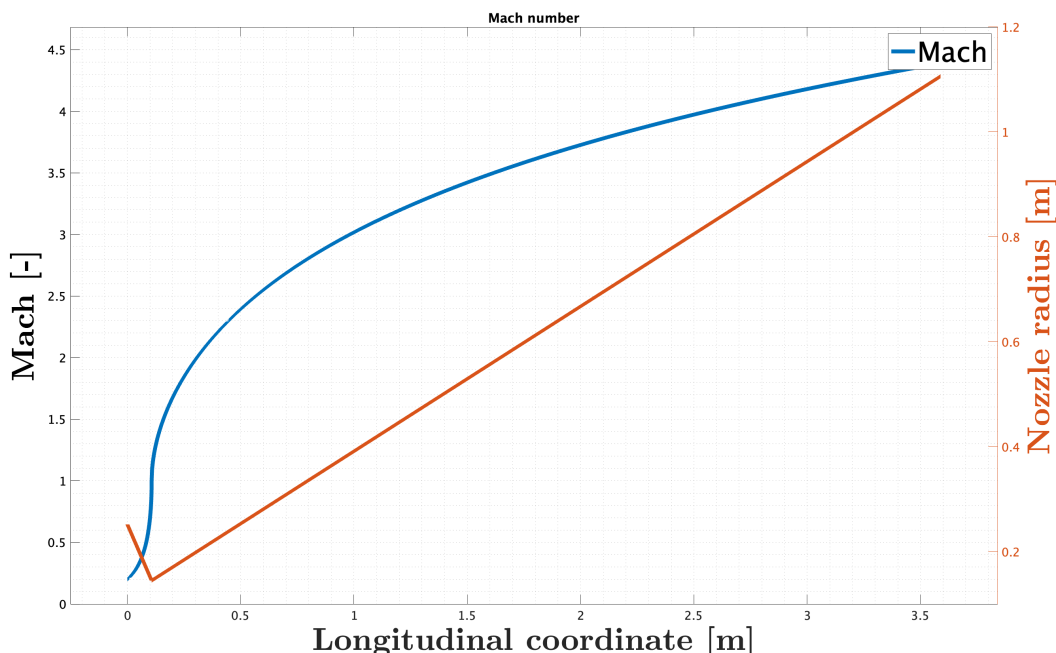


Figure 3.8



3.2.6 Combustion chamber and Injection Plate

3.2.6.1 Combustion chamber Dimensioning

In order to calculate the actual volume and length of the combustion chamber, a characteristic length should be chosen from *Space Propulsion Analysis and Design* [3]. There, for the couple Liquid O₂/Liquid H₂ the following range is reported:

$$0.76 \text{ m} < L^* < 1.02 \text{ m} \quad (3.5)$$

Thus, the mean value among the extremes is considered:

$$L^* = \frac{(1.02 + 0.76)}{2} = 0.89 \text{ m}$$

From that, the following formula yields the sought combustion chamber volume, length and the side area:

$$V_c = A_{throat} L^* = 0.0585 \text{ m}^3 \quad L_c = \frac{V_c}{A_c} = 0.2996 \text{ m} \quad A_{lat,c} = \pi D_c L_c = 0.4692 \text{ m}^3$$

As part of the thrust chamber assembly, the essential function of the injector head assembly is to uniformly inject liquid propellants into the combustion chamber at the proper oxidizer/fuel mixture ratio by either impinging propellant streams, swirling, shear mixing or other mechanical means of achieving maximum atomization.

3.2.6.2 Injection plate

The first step in injector design is to establish the injector flow-system geometry, which is the flow-controlling aspect of the injectors and consists in:

- the total injector element pattern;
- the individual orifice geometry;
- the flow-system geometry itself.

The purpose is to achieve high combustion performances and stable operations without affecting durability.

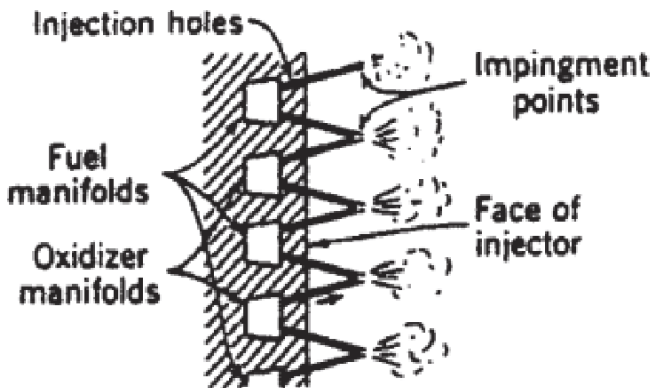


Figure 3.9: Double impinging stream pattern [2]

The launcher is assumed to be equipped with a double impinging stream pattern (as seen in figure Figure 3.9). Thus, the oxidant and the fuel are injected simultaneously at a certain angle and the collision is considered to be purely anelastic. Furthermore, the hypothesis of short-tube type with a rounded entrance orifice, such as the one shown in Figure 3.10, will be employed.

Short tube with rounded entrance $L/D > 3.0$		1.00	0.88
		1.57	0.90
		1.00	
		(with $L/D \sim 1.0$)	0.70

Figure 3.10: Short tube with rounded entrance [2]

From scientific literature [2] ,the typical dimension of an injection hole ($1h$) can be estimated, while its area and its discharge coefficient can be calculated as follows:

$$D_{1h} = 1.57 \text{ mm} \quad c_D = 0.9 \quad A_{1h} = \frac{\pi D_{1h}^2}{4} = 1.9359 \cdot 10^{-6} \text{ m}^2$$

With this data, it's possible to obtain the area of a single hole both for the oxidant and the fuel, considering a concentrated pressure loss ΔP_c for each injection hole:

$$\Delta P_c = 0.1 \cdot P_c = 11.5 \text{ bar}$$
$$A_{g,ox} = \frac{\dot{m}_{ox}}{c_D \sqrt{2\rho_{ox} \Delta P_c}} = 0.0060 \text{ m}^2 \quad A_{g,f} = \frac{\dot{m}_f}{c_D \sqrt{2\rho_f \Delta P_c}} = 0.0039 \text{ m}^2$$

And finally, the number of holes for each propellant can be found as:

$$N_{h,ox} = \frac{A_{h,ox}}{A_{1h}} = 3082 \quad N_{h,f} = \frac{A_{h,f}}{A_{1h}} = 2025$$



Knowing that the streams are simultaneous and injected in couples, both fluids need to have the same number of injectors, which is:

$$N_{inj} = \min(N_{h,ox}, N_{h,f}) = 2025$$

With this value, the following simple formula yields the cross-sectional area and diameter of a single oxidant and fuel injection hole:

$$A_{1h,ox} = \frac{A_{h,ox}}{N_{inj}} = 2.946 \cdot 10^{-6} \text{ m}^2 \quad A_{1h,f} = \frac{A_{h,f}}{N_{inj}} = 1.9352 \cdot 10^{-6} \text{ m}^2$$

$$D_{1h,ox} = \sqrt{\frac{4A_{1h,ox}}{\pi}} = 1.93 \text{ mm} \quad D_{1h,f} = \sqrt{\frac{4A_{1h,f}}{\pi}} = 1.57 \text{ mm}$$

To complete the injection plate design, appropriate values for the angles of injection for both the oxidant and the fuel must be calculated. Here, as previously stated, a totally anaelastic impact is assumed, which implies the conservation of momentum. Moreover, the considered nomenclature for the calculations is presented in Figure 3.11.

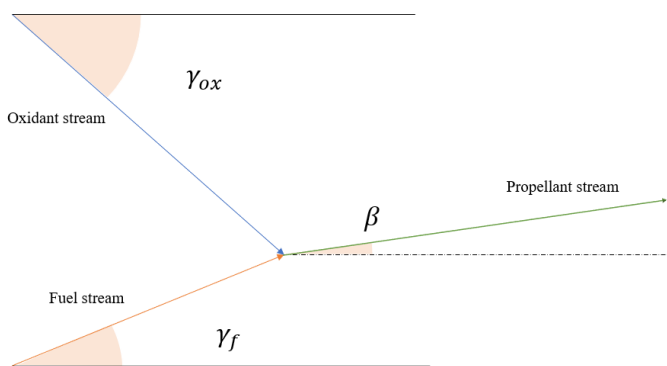


Figure 3.11: Reference angles

Where γ_{ox} , γ_f and β are the angle between the stream and the local horizon for the oxidant, the fuel and the total propellant stream, respectively.

From the previously obtained results, the velocity of the oxidant and the fuel stream can now be estimated as:

$$u_{ox} = c_D \sqrt{\frac{2\Delta P_c}{\rho_{ox}}} = 40.42 \frac{\text{m}}{\text{s}} \quad u_f = c_D \sqrt{\frac{2\Delta P_c}{\rho_f}} = 161.98 \frac{\text{m}}{\text{s}}$$

Assuming $\gamma_f = 50$ deg for the fuel stream and $\beta = 0$ deg (this last hypothesis is justified by the fact that it is convenient for the stream to be parallel to the combustion chamber's axis), the momentum conservation equation in y direction is:

$$\dot{m}_{ox} u_{ox} \sin(\gamma_{ox}) + \dot{m}_f u_f \sin(\gamma_f) = \dot{m}_p u_p \sin \beta = 0 \quad (3.6)$$



$$\gamma_{ox} = \gamma_f \sin^{-1} \left(\frac{\dot{m}_f u_f}{\dot{m}_{ox} u_{ox}} \right) = 35.83 \text{ deg}$$

The injection plate is therefore fully dimensioned.

3.2.7 Shear Coaxial Injectors

Once the jets impinge on one another, they form a liquid sheet which decomposes into smaller fragments and atomizes. The typical high mass flow rates establish within milliseconds a large enough amount of propellants. Their sudden reaction may lead to pressure peaks, which in turn may trigger combustion instabilities.

In order to provide an efficient atomization and mixing mechanism in order to lead to high performances and stability, Shear Coaxial Injectors (Figure 3.12) are used, a features of the latest version of the Vulcain engine [8].

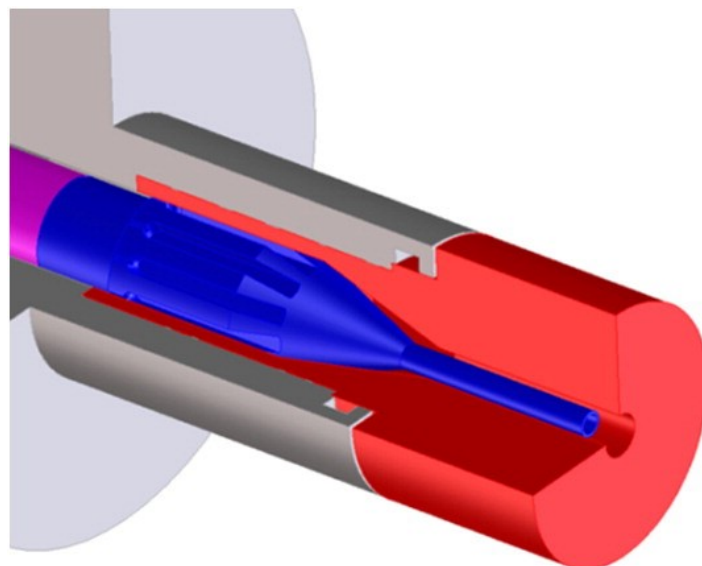


Figure 3.12: Shear coaxial injector assembly

Injector type	Shear Coaxial
Flow rate/element [kg/s]	0.55
Thrust/element [kN]	1.6

Table 3.8: Vulcan 2 Injector specifications table [14]

They consist of an inner duct from which the oxygen is injected into the combustion chamber and an external coaxial duct from which the LH2 is injected. They're mainly atomised and mixed by shear forces generated by the velocity differences between LOX and LH2. The restriction and the expansion afterwards introduce large scale turbulences in the liquid, which support the atomization.

In order to characterize the different operating points, non-dimensional quantities are employed. The velocity ratio v_R is the ratio between the fuel and the oxidizer stream velocities, giving a measure of the shear forces:

$$v_R = \frac{v_f}{v_{ox}}$$

Typical exit velocities of liquid propellants range between $10 \div 20 m/s$. The gaseous hydrogen enters the injector and is finally accelerated at the edge to velocities in the range of $250 \div 350 m/s$.

The momentum flux ratio J is defined as:

$$J = \frac{\rho_f v_f}{\rho_{ox} v_{ox}}$$

Both the velocity ratio and the momentum flux ratio are based on propellants temperatures and pressure measurements at injection conditions.

For shear coaxial injectors, the key parameters that characterize injector geometry are the recess length, taper angle and wall thickness of the liquid oxygen post, which is the inner tube of the coaxial injector.

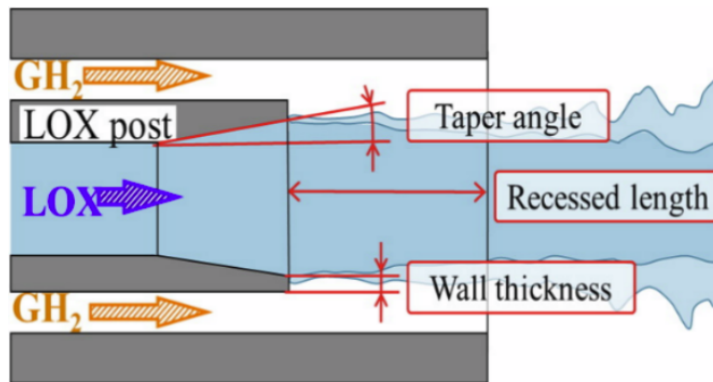


Figure 3.13: Shear coaxial injector functioning

The effects of the recessed length and taper angle of the liquid oxygen post on cryogenic coaxial jets have been experimentally investigated, suggesting that a recess of a certain length is required to improve the mixing of cryogenic coaxial jets. The effects of the liquid oxygen post exit taper on the mixing enhancement are, however, more significant than those of the recess at supercritical pressure, as in our case. They can be considered as the result of an increase in the J number.

The recessed length and the exit-taper angle of the LOX post can be varied within the ranges of $0 \div 6 mm$ and $5 \div 10$ deg, respectively, by replacing parts of the injector. The wall thickness at the LOX post exit decreases as the taper angle increases because the inner diameter of the LOX post in the non-tapered area is set to be the same in all cases.

The Vulcain 2's injector plate consists in 566 shear coaxial injectors.

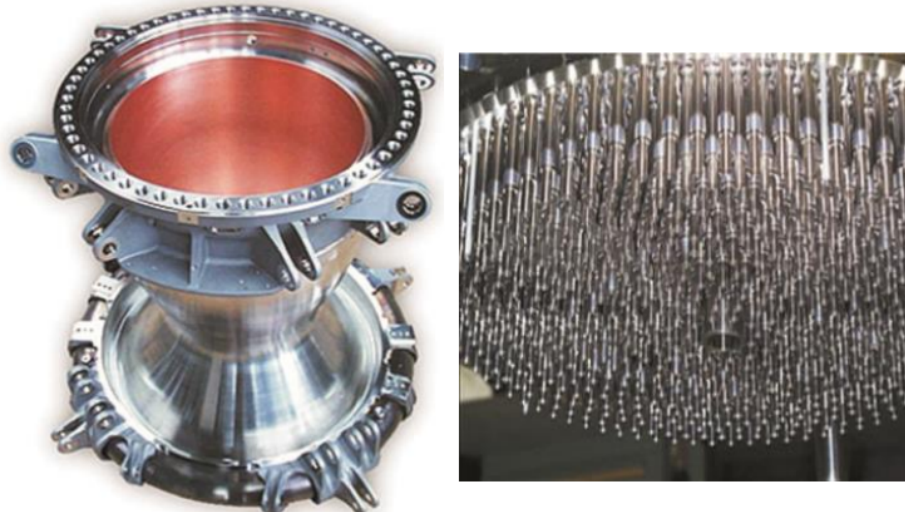


Figure 3.14: Combustion chamber of the Vulcain 2 engine (left) and injector assembly (right)

3.2.8 Helium Pressurization System

The oxidant and the fuel must be fed to the combustion chamber at a minimum guaranteed pressure, which is the combustion chamber pressure of 115 bar. To achieve this objective, two paths can be followed:

- Helium gas pressurization
- Turbopump system pressurization

It was decided to mathematically demonstrate the impossibility of the first option. To perform such activity, a hypothetical helium tank must be dimensioned. Helium' molar mass and specific heats values are:

$$M_{mol}^{He} = 4.0 \frac{\text{g}}{\text{mol}} \quad \gamma^{He} = 1.66$$

As shown in Figure 3.4, the oxidant and the fuel must flow through a certain length of pipes to arrive at the injection plate. As known from fluid dynamics, this causes a head loss. Since the actual length of the feeding system is unknown, the mentioned loss can be supposed as:

$$\Delta P_{feed} = 50 \text{ kPa}$$

It's also possible to obtain the dynamic pressure losses due to the fluid's kinetic energy, assuming the oxidant and fuel speed in the duct to 10 m/s :

$$v_{feed} = 10 \frac{\text{m}}{\text{s}}$$



$$\Delta P_{dyn,ox} = \frac{1}{2} \rho_{ox} v_{feed}^2 = 57 \text{ kPa} \quad \Delta P_{dyn,f} = \frac{1}{2} \rho_f v_{feed}^2 = 3.55 \text{ kPa}$$

Finally, the necessary pressures in the oxidant and fuel tanks can be found as:

$$P_{tank,ox} = P_c + \Delta P_c + \Delta P_{feed} + \Delta P_{dyn,ox} = 127.57 \text{ bar}$$

$$P_{tank,f} = P_c + \Delta P_c + \Delta P_{feed} + \Delta P_{dyn,f} = 127.036 \text{ bar}$$

The Helium gas tank pressure is considered to be a mean value of the oxidant and fuel tank pressures:

$$P_{tank,He} = \frac{P_{tank,ox} + P_{tank,f}}{2} = 127.30 \text{ bar}$$

In order to find the initial pressure of the pressurizing gas, its initial and final temperature must be hypothesized, whereas its final pressure is given, and it will be $P_{tank,fin} = P_{tank,He}$. In particular, it's possible to assume the final temperature of the tank between the freezing points and the boiling points of propellants:

$$T_{tank,fin} = 55 \text{ K} \quad T_{tank,in} = 90 \text{ K}$$

Given that the transformation is assumed to be adiabatic and reversible and helium to be calorically and thermally perfect, the isentropic relation for ideal gases allows to find the initial pressure of the tank like:

$$P_{tank,in} = P_{tank,fin} \left(\frac{T_{tank,in}}{T_{tank,fin}} \right)^{\frac{\gamma_{He}}{\gamma_{He}-1}} = 439.32 \text{ bar}$$

To find the helium mass and volume, an iterative method with an iteration criterion must be used. Each step j of the method involves the following equations:

$$M_{He,j} = \frac{P_{tank,fin}}{R} [V_{ox} + V_f + V_{He,j-1}] \quad \text{with} \quad V_{He,j} = \frac{M_{He,j}}{P_{tank,in}} \frac{R}{M_{mol,He}} T_{tank,in}$$

For every $j = 1, 2, \dots, \infty$. The stopping criterion is based on the relative residual:

$$\frac{M_{He,j} - M_{He,j-1}}{M_{He,j-1}} < tol$$

Where tol can be assumed as $tol = 0.02$. With just six iterations, a total mass of 99.03 tons and a volume of 416.33 m^3 of Helium are extrapolated. This demonstrates without any doubt that a helium-based pressurization system is unfeasible, because both the volume and the mass of the pressuring gas and relative tanks would be huge and totally unwieldy for the mission. A change in the pressurization system seems therefore necessary.



3.2.8.1 Turbopump system

Type	2-stage axial, transonic
Power rating	9.9 ÷ 20.4MW [14.1MW]
Speed	31800 ÷ 39800rpm [35500rpm]
Inlet pressure	60 ÷ 122bar
Outlet pressure	4 ÷ 7.5bar
Inlet temperature	770 ÷ 960K
Blade meanline diameter	0.24m

Table 3.9: LH₂ Turbine Specifications

Type	2-stage axial, transonic
Power rating	3.7 ÷ 6.6MW [5.1MW]
Speed	11300 ÷ 13700rpm [12600rpm]
Inlet pressure	40 ÷ 101bar
Outlet pressure	4.5 ÷ 7bar
Inlet temperature	770 ÷ 960K
Blade meanline diameter	0.32m

Table 3.10: LOX Turbine Specifications

Indeed, the Vulcain 2 engine pressurises the propellants by a turbopump system that is powered by a Gas Generator.

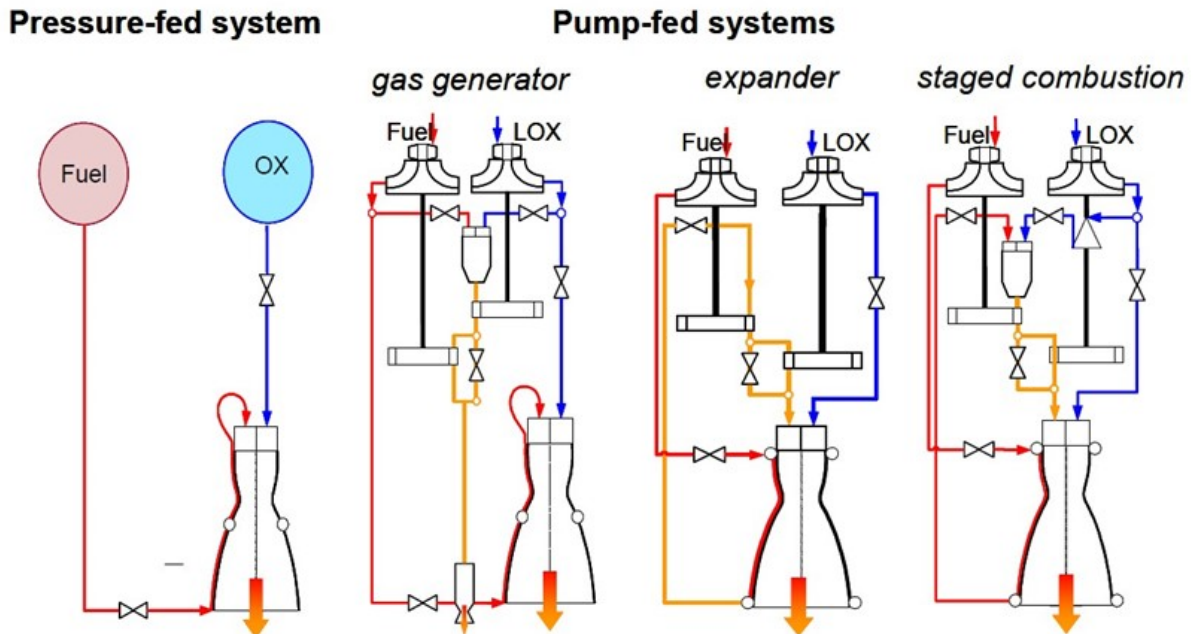


Figure 3.15: Schematic of the turbopump compression system of the Vulcain 2 engine



The Gas Generator is essentially a small combustion chamber and since its purpose the one of feeding energy to the turbines that drive the pumps, it gets said energy by the burning of a small fraction of the propellants themselves. In our case, it is home to a fuel rich combustion for the purpose of limiting the temperature at around 850 K to then ensure that the turbopump turbine's blades survive for enough time to complete the mission. The cycle schematics in figure Figure 3.15 show that the case characterized by the direct release of the turbine exhaust gases into the ambient is called "Gas Generator Cycle". In the case that they are fed together with the remainder of the propellants into the main combustion chamber, this cycle is called "Staged Combustion Cycle" [13].

T_{GG}	875	[K]
P_{GG}	10.1	[MPa]
O/F	0.9	[-]
$\dot{m}_{GG_{tot}}$	9.7	[kg/s]
LOX turbine Power	5.1	[MW]
LH ₂ turbine Power	14.1	[MW]
CEA calculations		
M	3.830	[kg/kmol]
Cp_{cg}	8.074	[kJ/kgK]
γ_{eg}	1.3677	[-]

Table 3.11: CEA Output table

Knowing the data on the right, we can easily calculate the OX and H₂ which pass through the gas generator:

$$\dot{m}_{GG_{H_2}} = \frac{\dot{m}_{GG_{tot}}}{OF + 1} = 5.1053 \frac{\text{kg}}{\text{s}} \quad \dot{m}_{GG_{OX}} = \dot{m}_{GG_{H_2}} \cdot OF = 4.5947 \frac{\text{kg}}{\text{s}}$$

The total turbines power is:

$$P_{turb,tot} = P_{turb,OX} + P_{turb,H_2} = 19.3 \text{ MW}$$

and temperature and pressure after expansion in the turbines:

$$T_f = T_{GG} - \frac{P_{turb,tot}}{\eta_t \cdot \dot{m}_{GG_{tot}} \cdot Cp_{cg}} = 624.84 \text{ K}$$

$$P_f = P_{GG} \cdot \left(\frac{T_f}{T_{GG}} \right)^{\frac{\gamma_{cg}}{\gamma_{cg}-1}} = 2.8865 \text{ MPa}$$

assuming the yield of the turbines $\eta_t = 0.98$.

Afterwards, we can calculate the thrust contribute given by the combust gasses with some assumptions. Since the combust gasses are injected in the nozzle at $\varepsilon_{entry} = 32$, we assume that the combustion gasses in the inlet are in throat sonic condition; by this point onwards, they expand as the exhaustion gasses do in the divergent. We also assume that



the regenerative cooling H₂ portion, which also enters the nozzle for the film cooling, is not present and it doesn't interfere with the throat conditions.

$$\varepsilon_{GG} = \frac{\varepsilon}{\varepsilon_{entry}} = 1.828$$

$$\varepsilon_{GG} = \frac{1}{M_{e,GG}} \left(\frac{2}{\gamma_{cg} + 1} \left(1 + \frac{\gamma_{cg} - 1}{2} M_{e,GG}^2 \right) \right)^{\frac{\gamma_{cg} + 1}{2 \cdot (\gamma_{cg} - 1)}}$$

By inverting this formula the exit mach number is found:

$$M_{e,GG} = 2.0742$$

Likewise the exit pressure $P_{e,GG}$ of the exhaust gases at the end of the nozzle can be calculated from the following expression:

$$\frac{1}{\varepsilon_{GG}} = \left(\frac{\gamma_{cg} + 1}{2} \right)^{\frac{1}{\gamma_{cg} - 1}} \left(\frac{P_{e,GG}}{P_f} \right)^{\frac{1}{\gamma_{cg}}} \sqrt{\frac{\gamma_{cg} + 1}{\gamma_{cg} - 1} \left(1 - \left(\frac{P_{e,GG}}{P_f} \right)^{\frac{\gamma_{cg} - 1}{\gamma_{cg}}} \right)}$$

$$P_{e,GG} = 3.3036 \cdot 10^5 \text{ Pa}$$

Through the relationship provided by the adiabatic-isoentropic transformation, we're able to obtain the exit velocity:

$$v_{e,GG} = \eta_t \cdot M_{e,GG} \cdot \sqrt{\gamma_{cg} \cdot R_{GG} \cdot T_f \cdot \left(\frac{P_{e,GG}}{P_f} \right)^{\frac{\gamma_{cg} - 1}{\gamma_{cg}}}} = 2069 \frac{\text{m}}{\text{s}}$$

Vandenkerckhove function helps out when it comes to calculate the throat cross sectional area:

$$\Gamma_{cg} = \sqrt{\gamma_{cg} \cdot \left(\frac{2}{\gamma_{cg} + 1} \right)^{\frac{\gamma_{cg} + 1}{\gamma_{cg} - 1}}} \Rightarrow A_{t,GG} = \dot{m}_{GG,tot} \cdot \sqrt{\frac{R_{GG} \cdot T_f}{\Gamma_{cg} \cdot P_f}} = 0.0058 \text{ m}^2$$

and the external area by consequence: $A_{e,GG} = \varepsilon_{GG} \cdot A_{t,GG} = 0.0105 \text{ m}^2$

We can now calculate the contribute of thrust given by the gas generator combust gases at an optimum altitude of 10000 m:

$$T = \dot{m}_{GG,tot} \cdot v_{e,GG} + (P_{e,GG} - P_e) \cdot A_{e,GG} = 23.331 \text{ kN}$$

Disregarding this increase in thrust, but still considering the 9.7 kg/s burned by the pre-burner, the specific impulse can be found as: $I_{sp} = \frac{T_{cc}}{(g_0 \cdot (\dot{m}_p + \dot{m}_{GG,tot}))} = 423.7998 \text{ s}$

While, adding the increase in thrust we just calculated with our approximations, the specific impulse becomes $I_{sp} = 431.0133 \text{ s}$ resulting in a gain of 7.21 s.



3.3 Cooling system

A major concern is the injector/chamber wall interaction: as clearly visible on the wall of the combustion chamber liner of the Vulcain engine shown in Figure 3.16, it causes the so called “blanching”. Injection of a coolant film is a method to cope up with this problem.

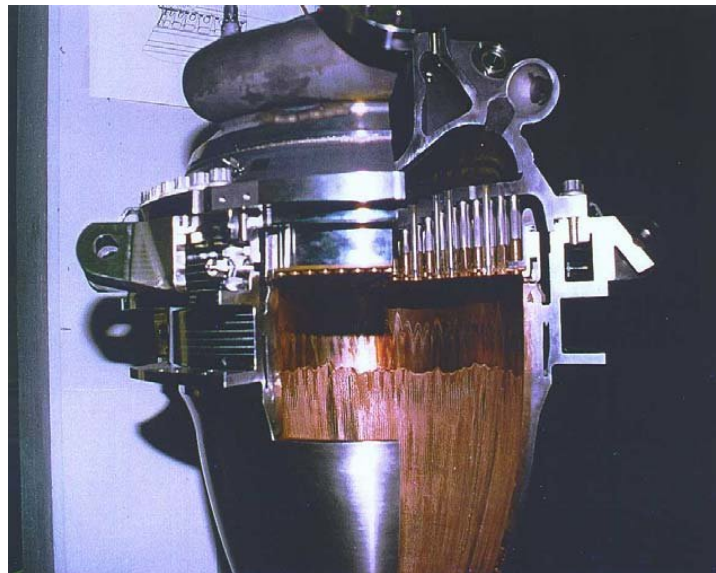


Figure 3.16: Cutout section of the combustion chamber

High temperature differences between the hot combustion gases and the chamber walls yield to extreme high heat flux levels and temperature gradients through chamber and nozzle. Indeed, rocket engine cooling is necessary for mechanical considerations: enough heat has to be absorbed to keep the walls at a sufficiently low temperature, so that the wall material is strong enough to withstand the stresses imposed by the fluid pressure, thermal gradients, and other loads.

Symbol	Meaning	Value	Unit
P_r	Prandtl number	0.5512	[–]
μ	Viscosity	$1.0698 \cdot 10^{-4}$	[Pa · s]
k_w	Copper coefficient of thermal conductivity	$15.3848 \cdot 10^{-1}$	[$\frac{W}{m \cdot K}$]

Table 3.12: Cooling operational data table

3.3.1 Regenerative cooling

Combustion temperature control is firstly achieved by a flow of LH₂ in the cooling channels within the combustion chamber wall. This thin copper alloy wall, just 1.5 mm thick, separates the combustion temperatures from the -239°C to -150°C LH₂ cooling flow. Gaseous hydrogen is used to cool the upper part of the nozzle while flowing through helical, rectangular cooling channels, which have the function of heat-exchanger. The heat absorbed by the coolant is not wasted, rather the coolant is directly injected in the combustion chamber. Thus, it increases the initial energy content of the propellant prior to injection, slightly raising the specific impulse ($0,1 \div 1,5\%$).

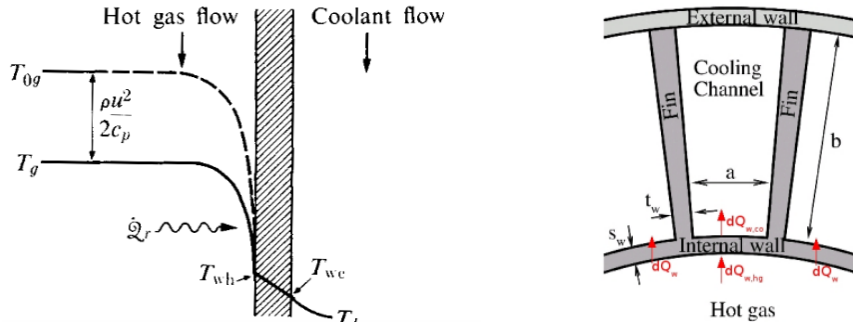


Figure 3.17: Cooling Jacket Schematic

This first kind of cooling is called regenerative cooling [17], which requires sufficient pressure to force the coolant through the cooling passages, which the turbopumps system are able to provide.

The hot-gas flow is formulated on the basis of a one-dimensional isentropic expansion (i.e., one-dimensional flow model with variable area of the cross section). For steady conditions and assuming a one-dimensional cooling jacket model, the heat transfer balance is:

$$Q_{hg,w} = Q_w = Q_{w,c} \quad (3.7)$$

where $Q_{hg,w}$ is the heat flux from the hot gas to the wall, Q_w is the heat flux through the wall and $Q_{w,c}$ is the heat flux from the wall to the coolant flow. Let us analyze these terms.

3.3.1.1 Heat flux from the wall to the coolant flow

For simplification purposes the conduction between the outside wall of the chamber and the coolant flow is assumed perfect, meaning that the inside wall temperature is equal to the coolant flow temperature:

$$T_{w,out} = T_c = 123.15 \text{ K}$$

This is a pretty severe assumption but, since the highest possible coolant temperature T_c is used (as mentioned before this could range from 34.15 K to 123.15 K), it is assumed to be acceptable.

3.3.1.2 Heat flux through the wall

The heat flux by conduction can be expressed as:

$$Q_w = \frac{k_w}{s_w} (T_{w,in} - T_{w,out}) \quad (3.8)$$

where $T_{w,in}$ and $T_{w,out}$ are the wall temperature at the hot-gas side and coolant side respectively, k_w is the wall thermal conductivity and s_w is the internal wall thickness. The effect of curvature is neglected since the wall thickness s_w is considered small if compared to the nozzle radius r .



3.3.1.3 Convective wall heat

The convective wall heat flux $Q_{hg,w}$ is expressed as the product of a heat transfer coefficient h and a driving potential which represents the difference of the energy levels between free stream and wall.

For a high-speed flow (such as the hot-gas case) the driving potential is based upon the recovery temperature:

$$Q_{hg,w} = h \cdot (T_{aw} - T_w) \quad (3.9)$$

where T_{aw} is the adiabatic wall temperature (or recovery temperature) and T_w is the wall temperature at the hot-gas side ($Q_{hg,w}$ is considered positive if the heat flux exits the hot-gas). The adiabatic wall temperature can be expressed as:

$$T_{aw} = T \cdot \left(1 + r \frac{\gamma - 1}{2} M^2 \right)$$

where M is the free stream Mach number, T is the free stream temperature, γ is the specific heats ratio and r , the recovery factor, is a value related to the Prandtl number found as $r = P_r^{\frac{1}{3}}$.

For the convective coefficient h the Bartz relation is used, in particular:

$$h = \frac{0.026}{D^{0.2}} \left(\frac{\mu^{0.2} \cdot c_p}{P_r^{0.6}} \right)_0 (\rho u)^{0.8} \cdot \sigma$$

where D is local diameter at the station of the nozzle of interest, μ is the flow viscosity, c_p is the perfect gas specific heat, P_r is the flow's Prandtl number, ρu is the product of the flow's density and velocity at the station of interest and σ is defined as:

$$\sigma = \frac{1}{\left[\frac{1}{2} \frac{T_w}{T_0} \left(1 + \frac{\gamma-1}{2} M^2 \right) + \frac{1}{2} \right]^{0.68} \cdot \left[1 + \frac{\gamma-1}{2} M^2 \right]^{0.12}}$$

Finally the equation for h can be put in a form suitable for rocket nozzle computations by evaluating ρu in terms of c^* and the ratio $\frac{A_*}{A}$ where A_* is the cross-sectional area at the nozzle throat:

$$h = \left[\frac{0.026}{D_*^{0.2}} \left(\frac{\mu^{0.2} \cdot c_p}{P_r^{0.6}} \right)_0 \left(\frac{P_c}{c^*} \right)^{0.8} \right] \left(\frac{A_*}{A} \right)^{0.9} \cdot \sigma$$

This equation is the final form proposed by Bartz and it is one of the most used approaches to estimate the nozzle convective heat transfer. Note that the factor in the $[,]$ brackets is a constant through the nozzle, leaving only $\frac{A_*}{A}$ and σ to be evaluated at each station.

3.3.1.4 Balance solution

The only thing left to do is explicit the balance and solve it. Using equations 3.7, 3.8 and 3.9 gives:

$$0 = h \cdot (T_{aw} - T_w) - \frac{k_w}{s_w} (T_w - T_{w,out})$$

where $T_{w,in}$ has been set equal to T_w .

The balance is a function of T_w only and thus can be solved numerically using MatLab's `fsove` that yields figure 3.18.

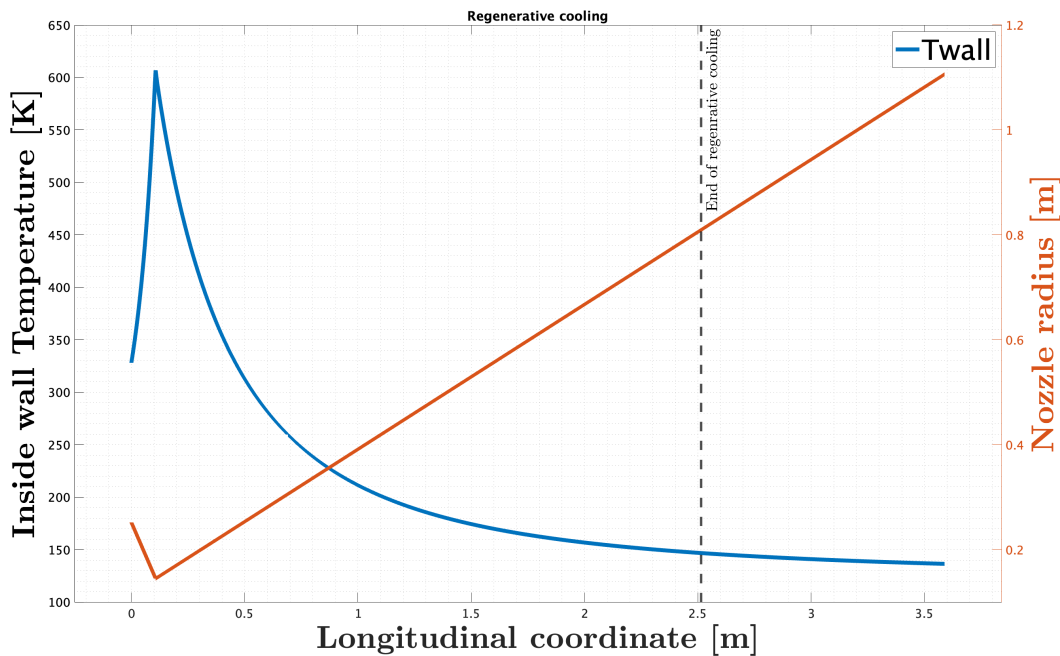


Figure 3.18: Regenerative cooling temperature graph

3.3.1.5 Film cooling

Film cooling is used for the Vulcain 2 cooling system in combination with the dump cooling: at a nozzle area expansion ratio of $\varepsilon = 32$ the hydrogen is injected with supersonic velocity as a film to protect the lower section of the nozzle from heat impact of the accelerated combustion gases. There are two ways to dump the hydrogen in the nozzle, in the direction of the flow and perpendicular to the divergent wall. Data have shown that dumping in the direction of the flow augments the cooling efficiency by around 30%. [7]

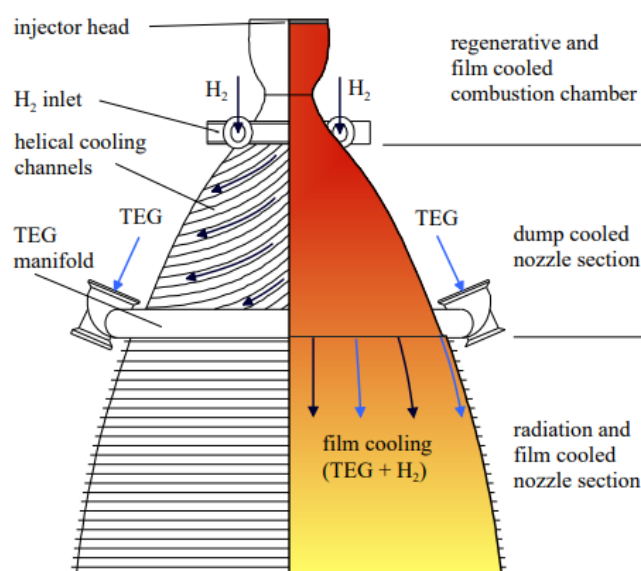


Figure 3.19: Cooling design of combustion chamber and nozzle

Additional to the dumped hydrogen, the Turbine Exhaust Gases (TEG) with a mass flow rate of approximately 10 kg/s are injected as a film at almost the same position. To provide equal circumferential coolant distribution, the TEG is guided by two pipes from the upper part of the engine alongside the upper nozzle part, as visible in Figure 3.19. Generally, the film cooling provides to reduce the highest temperature by 1800 K. That grants a reduction of more than 50% as compared to the case without fluid injection where temperatures reach 3000 K.

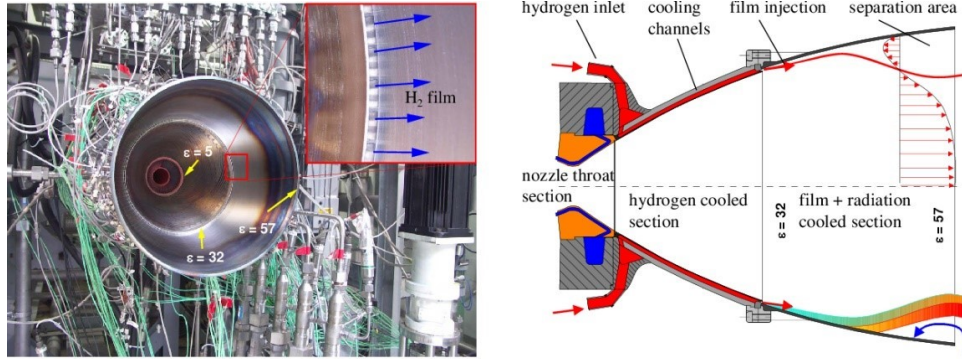


Figure 3.20: PKE with Nozzle extension (left) and Nozzle extension schematic (right)

To investigate the film cooling effectiveness η downstream the point of injection the following definition has been used [16]:

$$\eta = \frac{T_w - T_{cc}}{T_2 - T_{cc}}$$

where:

T_w	Local nozzle temperature in nozzle skirt
T_2	Film injection temperature
T_{cc}	Temperature of the combustion chamber

Table 3.13: Temperature table

The film coolant mass flow rate has been varied in the range of $\dot{m}_{cool}/\dot{m}_{core} = 3.4 \div 4.1\%$. A higher film mass flow rate results in a lower local wall temperature and increased film effectiveness. At the injection point the cooling efficiency is 1, meaning that both the wall temperature and the coolant temperature have the same value. Further downstream, a mixing of the hot combustion gases and the injected hydrogen film occurs, and the local film effectiveness is reduced. However, 150mm downstream the film injection the effectiveness η is still in the range of 90%.

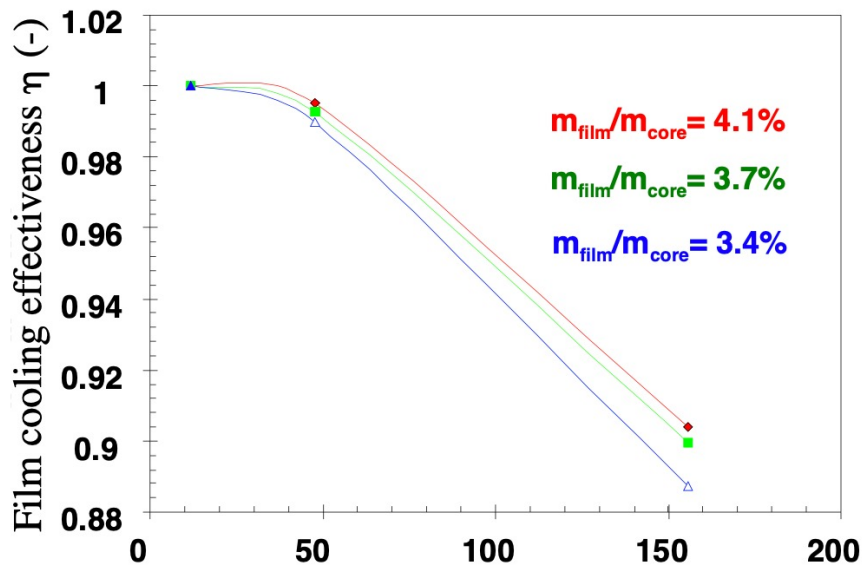


Figure 3.21: Film cooling defectiveness chart

An increased mixture ratio gives a slightly higher film cooling effectiveness within the investigated range of film mass flow rates.



4 James Webb Space Telescope

The Ariane V launcher was used in the first two decades of the 20th century to deliver very different payloads in various orbits. Among the more than 100 missions for which this type of launcher has been used, one of the most important remains Mission 112 which launched from Ariane's Spaceport in Korou, French Guiana, on December 25, 2021. The primary goal of Mission 112 was to orbit the James Webb Space Telescope (JWST) in the Sun-Earth L2 Lagrange point. In order to replace the Hubble Space Telescope, NASA, the European Space Agency, and the Canadian Space Agency developed the JWST, an infrared space telescope. The observatory, which is the space segment component of the JWST compound, is itself composed of three different elements: the Integrated Science Instrument Module (ISIM); the Optical Telescope Element (OTE); and the shuttle system, which includes the shuttle, or Spacecraft Bus, and the sunshield.

We will go deeper into the Spacecraft Bus Propulsion System in this chapter to learn more about the thruster designs deployed on the James Webb Space Telescope and their intended uses [15].

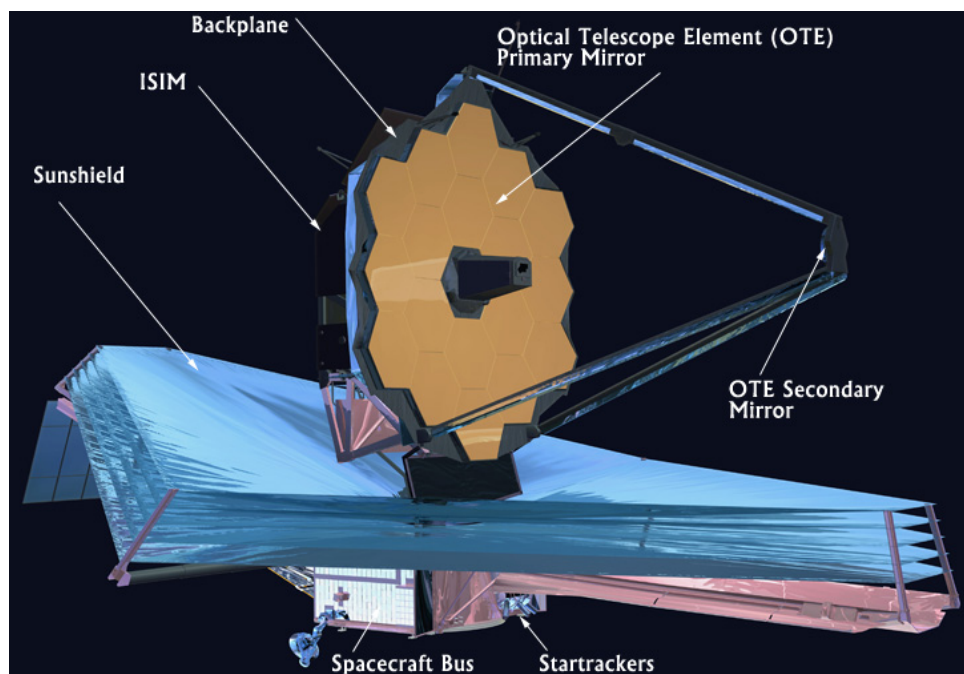


Figure 4.1: Schematic of the JWST



4.1 Characterization of the stage

4.1.1 Characteristics

Data	Value
Hydrazine Volume	$159L$
N ₂ O ₄ Volume	$79.5L$
Mass (Bus + Telescope)	$6161, 4(5.811, 4 + 350)Kg$
MCC-1a Burn Time	$11425s$
MCC-1b Burn Time	$2622s$
MCC-2 Burn Time	$1301s$

Table 4.1: Table of specifications

4.1.2 Introduction

The propulsion system of the JWST consists of two different sets of thrusters.

The first system is called Secondary Combustion Augmented Thruster (SCAT)s and was used as the main propulsion during Mid-course Corrections (MCC) maneuvers. SCATs are bi-propellant liquid thrusters using hypergolic fuel from two separate tanks. Two separate pairs of SCATs were mounted on the spacecraft: the SCAT 1 used for the MCC-1a and MCC-1b maneuvers with its SCAT 2 redundancy copy, and the SCAT 3 used for the MCC-2 maneuver with its SCAT 4 redundancy copy. The second system consists of eight Dual Thrusters Modules (DTMs), each of which is composed of a primary thruster and a redundant thruster. The thrusters used are Monopropellant Rocket Engines (MRE-1), where the number 1 indicates the thrust produced by each individual thruster, which corresponds to about 4.5 N. MRE-1s are monopropellant liquid thrusters that use hydrazine, taken from the same tank as SCATs, as fuel without any oxidizer. The eight DTMs are divided into two sections: one section comprising DTMs numbered 1 to 4 aligned with the J3 axis of the observatory are used for roll and pitch control; the other section comprising DTMs numbered 5 to 8 directed radially with respect to the J3 axis are used for yaw control.

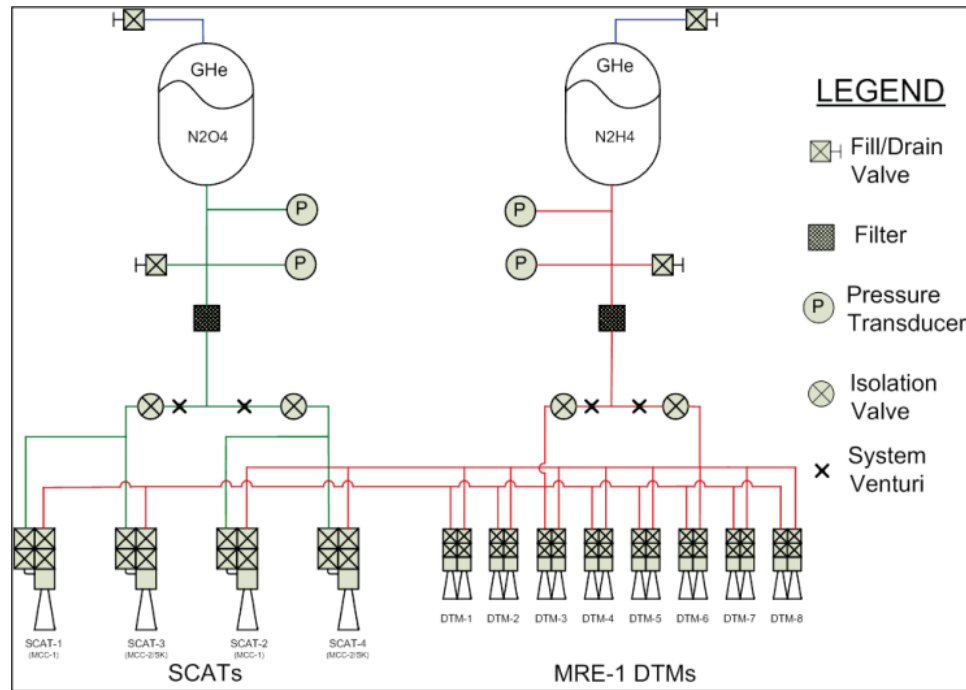


Figure 4.2: Picture of the JWST Propulsion System

As seen in Figure 4.2, the propulsion system is built on two main lines, one for each tank. Both tanks are pressurized and filled with Gaseous Helium (gHe) as the tanks release oxidizer and fuel into the system. Furthermore, both tanks have a filling valve detached from the main line to fill the tanks with gHe. The oxidizer line is limited to the SCATs as they are the only motors that use the oxidizer.

The main oxidizer line is composed of two pressure transducers for redundancy to always have a pressure reading inside the line; a filling/draining valve to refill the line with oxidizer and eventually relieve the line in eventual emergencies; a filter is then placed to remove any impurities before going in the actual thrusters as not to damage them; the main line then splits in two lines, one for each couple of SCATs. Before reaching the thrusters, the line passes through a Venturi system to reduce the pressure in the line and an isolation valve straight after to close the line when needed. The fuel line supplies both the SCATs and the DTMs and has almost the same schematics as the oxidizer line. The difference appears after the line splits into two distinct lines: both lines, as seen with the oxidizer, refuel separately a couple of SCATs each, but both lines feed to all 8 MRE-1 thrusters each in order to create enough redundancy [15].

4.2 Characterization of the propellant

4.2.1 Hydrazine

Differently from the second stage of the Ariane V launcher, these two thrusters use Hydrazine (N_2H_4) as fuel. Hydrazine is a simple pnictogen hydride that appears as a clear, colourless liquid with an odour similar to that of ammonia. Hydrazine is thermodynamically unstable with respect to decomposition into the elements and is exothermic when decomposed. It quickly decomposes catalytically and also decomposes thermally in the



vapour phase if heated to a high enough temperature. In either case, decomposition is accompanied by the release of considerable amounts of energy. Although hydrazine is easy to decompose, the initiation energy required is high enough that it can be handled quite safely. It is not shock-sensitive and can be heated to approximately 260 °C before thermal decomposition becomes a problem. It should be noted, however, that many materials begin to act as catalysts well below 260 °C; therefore, a more practical limit is about 177 °C. Mixtures of air and hydrazine vapour are extremely flammable, and care must be taken to exclude air from any hydrazine system. Mixing hydrazine with an oxidising agent such as dinitrogen tetroxide, N₂O₄, creates a hypergolic mixture, a mixture so powerful no ignition is required.

As the fuel burns, three reactions take place, decomposing hydrazine into ammonia, nitrogen, and hydrogen gases. Despite its high toxicity and volatility, hydrazine has been used as a propellant for spacecraft's propulsion systems since the 1960s. Europe has decided to ban completely the use of hydrazine by 2025 to stop the pollution and health hazards resulting from its production and use.

4.2.2 Dinitrogen Tetroxide

Dinitrogen Tetroxide (N₂O₄), commonly referred to as Nitrogen Tetroxide (NTO) is the chemical compound N₂O₄. Dinitrogen tetroxide is a powerful oxidizer that acts as a hypergolic upon contact with various forms of hydrazine, which has made the pair a common bipropellant for rockets. Nitrogen tetroxide is thus used as an oxidising agent in important rocket propellants because it can be stored as a liquid at room temperature. NTO is often used with the addition of a small percentage of nitric oxide, which inhibits stress-corrosion cracking of titanium alloys, avoiding corrosion and wear in the tanks. In this form, propellant-grade NTO is referred to as Mixed Oxides of Nitrogen (MON). In recent years, most spacecraft have pivoted to using MON instead of NTO.

4.3 Secondary combustion augmented thrust

The Secondary Combustion Augmented Thruster (SCAT) is a set of thrusters in JWST's propulsion system, used to maintain the orbit of the observatory. This type of thruster is composed of two connected reaction chambers and uses the same oxidizer to both cool the thruster chamber, whereby the oxidizer is transformed to a gaseous phase, and, in the gaseous phase, as the second propellant for the bipropellant mode of operation. Liquid propellant fuel, hydrazine, is fed into the first chamber, where it reacts with a catalyst and enters the gaseous phase in an exothermic reaction, thereby heating the chamber walls. The reaction propellant gas is propelled by the reaction into a second chamber. Liquid propellant oxidizer, N₂O₄, is fed through a heat exchanger surrounding the thruster and thereby cools the unit, and the associated energy absorbed by the oxidizer transforms the liquid oxidizer to the gaseous state. The gaseous oxidizer is then routed into the second chamber, where it mixes with the gaseous propellant fuel entering from the first chamber and reacts with the propellant to create thrust. Using the two propellants, SCAT produces an I_{sp} of about 315 s to 325 s seconds.

Using the thermal energy to perform the work of vaporising the liquid oxidizer instead of the alternative of radiating that thermal energy into space and using an alternative va-



porisation procedure for the oxidizer obviously somewhat enhances the efficiency of the propulsion process used in SCAT thruster

The cooling effect inherent in SCAT bipropellant mode of operation raises an additional factor of importance for some spacecraft missions: durability. The inherent cooling that occurs in the normal operation of SCAT engine suggests a longer operational life in comparison to other engines. SCAT is noted as having dual-mode capability. It is shown to operate in a bipropellant mode and, alternately, in a monopropellant mode. It is now realised that a simple SCAT bi-modal thruster can operate in either a bipropellant mode and achieve an I_{sp} of over 315 s seconds, or, alternatively, can operate in a monopropellant mode and achieve an I_{sp} of about 325 s seconds [18].

4.4 Dual Thruster Module

Dual Thrusters Modules (DTMs), is a secondary propulsion module used on the JWST. Each module is composed by two MRE-1 thrusters, a main thruster and its redundancy copy, and it's used for momentum unloads. The thrusters are oriented so that torque can be applied in roll, pitch, or yaw control axes and when fired the applied torque provides the necessary change to the angular momentum of the reaction wheels. The MRE-1 thrusters are monopropellant 1 – $lb\text{f}$ (4.4 N) thrusters. Monopropellant engines generate thrust by liquid hydrazine flowing through an open propellant valve into a catalytic decomposition chamber where the propellant goes through a highly energetic decomposition process and the hot decomposition gases are then accelerated through a converging-diverging nozzle. The most common catalyst is granular alumina (aluminum oxide) coated with iridium. Granular alumina is a spontaneous catalyst, that is, hydrazine decomposes on contact with the catalyst. The decomposition is highly exothermic and produces a 1000 °C gas that is a mixture of nitrogen, hydrogen and ammonia. The main limiting factor of the monopropellant rocket is its life, which mainly depends on the life of the catalyst. The catalyst may be subject to catalytic poison and catalytic attrition which results in catalyst failure. The thruster is fired when the computer sends direct current through a small electromagnet that opens the poppet valve [19].

4.5 Monopropellant Catalyst Thrusters

The chemical reaction that creates thrust occurs in a finite environment called a reaction chamber. The hydrazine-based catalytic decomposition chamber consists of an injector and a catalyst bed enclosed in a suitable container. The main purpose of the injector is to atomize the liquid hydrazine and to distribute it to the catalyst bed as uniformly as possible. A second objective is to place the maximum amount of catalyst in contact with the hydrazine in as short a time as possible to minimize the start transient time. The performance of monopropellant hydrazine reactors can be measured with the usual rocket parameters of characteristic exhaust velocity c^* and specific impulse I_{sp} . However, there exists a single parameter, unique to monopropellant hydrazine, to completely specify the performance. This parameter is the amount of ammonia remaining in the decomposition products as these gases leave the catalyst bed. More commonly, one minus this quantity, or the amount of ammonia that has been dissociated, is used.

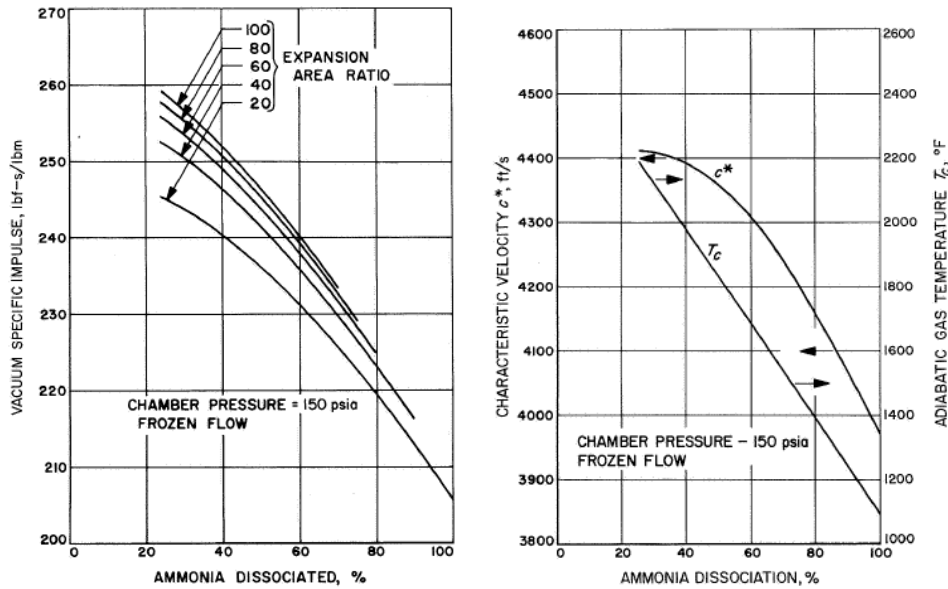


Figure 4.3: Theoretical I_{sp} -NH3% Graph (left) and Theoretical c^* -NH3% Graph (right)

The hydrazine monopropellant catalyst thrusters are usually divided into three distinct categories:

- Continuously operated thrust producing devices.
- Intermittently operated thrust producing devices.
- Gas generators.

The MRE-1 Thrusters used in the JWST secondary propulsion belong to the intermittently operated thrust producing devices category as these thrusters are used mainly to change the momentum of the reaction wheels when needed. Pulse operations are characterized by very short periods of propellant flow to the reaction chamber, as well as by many starts and stops of the reactor operations. Pulse operation of a hydrazine monopropellant reactor creates a set of problems not encountered during continuous operations. Very short start and shutdown transients are generally required over a varying range of environmental conditions. Reproducibility is often more important than a short pulse requirement, especially reproducibility of the impulse centroid. One common approach to shortening the start transient is to increase the bed loading. But this approach can drastically affect the catalyst loss rate. Repeated pulses also appear to be more detrimental to the catalyst than continuous operation. These problems have to be dealt with one at the time to come to a concrete solution [19].

4.5.1 Start Transient

The start transient is usually described in terms of the time from the valve-on electrical signal until 90% of the final steady-state or thrust is reached. Included in this overall response time are the valve opening time, the time to fill the propellant feed system, the time between the introduction of hydrazine to the catalyst bed and the beginning of the decomposition reaction, and the time required to generate enough gas to raise the chamber



pressure to nearly its final value. The valve actuation and feed system fill times can, of course, be reduced by proper design. The ignition delay and the rise time are strongly affected by the injection scheme, the catalyst bed geometry, the history of the catalyst, and the initial catalyst and propellant temperatures. The majority of the injector schematics achieve a total response time in the order of 10 ÷ 20 ms for a warm catalyst bed, and several can approach this time for an initial bed temperature of less than 40 °C. The catalyst bed geometry for pulsed reactors is dominated by the need to place a maximum catalyst surface area adjacent to the injector. This requirement presents no problem for low-thrust devices since a small sized granular catalyst is sufficient for this purpose. The internal surface area of the catalyst can decrease significantly during the course of its life due to high temperatures. This change in area significantly affects the start transient only in intermittently operated thrusters as the bed is allowed to cool below 150 °C before firing again. As seen in Figure 4.4, the initial temperatures of the catalyst bed and the propellant have a very strong influence on the start of the transient.

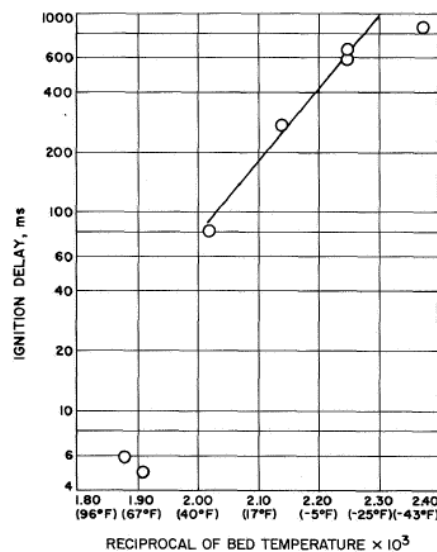


Figure 4.4: Ignition delay vs bed temperature

The temperature of the catalyst bed and propellant also affects the shape of the pulse. For applications where a long series of pulses are required, the error from the non-reproducibility introduced by the first pulses becomes negligible, as seen in Figure 4.5. In recognition of the difficulties involved in creating a pulse series and making the pulses match, the reproducibility requirement is often written in terms of later pulse.

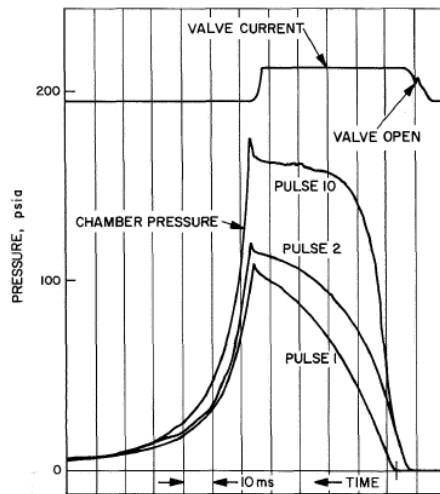


Figure 4.5: Characteristic response vs chamber pressure

4.5.2 Catalyst Bed Lifetime

The physical loss of catalyst can be a severe problem for pulsing thrusters. Many periods of short operations impose a more severe environment than an equivalent amount of continuous operation. Several companies have built reactors capable of several hundred thousand pulses with a total on-time on the order of 50 000 s (14 h). These reactors generally operate at low bed loadings. High bed loading is certainly a more stringent condition. A long train of pulses is a much less difficult requirement than many starts with a cold bed, a condition most likely to be affected by catalyst degradation. To summarise, it is possible to achieve long lifetimes for pulsed reactors. Long-life requirements and severe operating conditions require careful design and the use of more sophisticated catalyst retention techniques.

4.5.3 Heat Transfer to the Feed System

The system has to be designed so as to severely limit the quantity of heat conducted to any region where stagnating fuel might be present. Monopropellant hydrazine thrusters usually operate without any cooling, with the chamber that can easily reach temperatures of over 1000 °C. The heat produced in the chamber may be conducted into the feed system, this can represent a serious problem in pulsed thrusters as during the periods of no propellant flow it is possible to transfer enough heat to the upstream side of the propellant valve to locally decompose the hydrazine. The best solution to solve this problem is to thermally isolate the critical parts of the liquid system from the chamber and catalyst bed and to make sure that there are no parts of the feed system where hydrazine is seated while stagnant.



Bibliography

- [1] Oscar Biblarz George P. Sutton. *Rocket Propulsion Elements, ninth edition*. John Wiley and Sons Inc, 1949. ISBN: 9781118753651.
- [2] W. Nurick G.Gill. *Liquid rocket engine injectors*. NASA, 1976. ISBN: 76N30284.
- [3] G.N. Henry e W.J. Larson R.W. Humble. *Space Propulsion Analysis and Design*. McGraw-Hill Higher Education, 1995. ISBN: 9780070313200.
- [4] CNES. *Technical features of the Ariane 5*. URL: <https://ariane5.cnes.fr/en/technical-features-0>.
- [5] Antony RuizD. Coulon. *Unsteady Numerical Simulations of Transcritical Turbulent Combustion in Liquid Rocket Engines*. URL: https://www.researchgate.net/publication/281598880_Unsteady_Numerical_Simulations_of_Transcritical_Turbulent_Combustion_in_Liquid_Rocket_Engines.
- [6] D. Coulon. *Vulcain-2 Cryogenic Engine Passes First Test with New Nozzle Extension*. URL: <https://www.esa.int/esapub/bulletin/bullet102/Coulon102.pdf>.
- [7] O. J. Haidn D. I. Suslov R. Arnold. *Convective and Film Cooled Nozzle Extension for a High Pressure Rocket Subscale Combustion Chamber*. URL: <https://core.ac.uk/download/pdf/11140342.pdf>.
- [8] Dustin Davis and Bruce Chehroudi. *Shear-Coaxial Jets from a Rocket-Like Injector in a Transverse Acoustic Field at High Pressures*. URL: <https://arc.aiaa.org/doi/10.2514/6.2006-758>.
- [9] ESA. *Ariane 5 ECA*. URL: https://www.esa.int/Enabling_Support/Space_Transportation/Launch_vehicles/Ariane_5_ECA2.
- [10] ESA. *Boosters (EAP)*. URL: https://www.esa.int/Enabling_Support/Space_Transportation/Launch_vehicles/Boosters_EAP.
- [11] ESA. *Webb's Ariane 5 gains upper stage*. URL: https://www.esa.int/ESA_Multimedia/Images/2021/11/Webb_s_Ariane_5_gains_upper_stage3.
- [12] Ariane Group. *Ariane 5 goes down in history with successful launch of Webb*. URL: <https://www.arianespace.com/press-release/ariane-5-successful-launch-webb-space-telescope/>.
- [13] O. Haidn. *Advanced Rocket Engines*. URL: <https://www.semanticscholar.org/paper/Advanced-Rocket-Engines-Haidn/05951e233ae8e2fb25709e1da7a7d2cc9a17a965>.
- [14] Susumu Teramoto Hiromi Tani and Koji Okamoto. *Effects of Injector Geometry on Cryogenic Shear Coaxial Jets at Supercritical Pressures*. URL: https://www.researchgate.net/publication/273188170_Effects_of_Injector_Geometry_on_Cryogenic_Shear_Coaxial_Jets_at_Supercritical_Pressures.
- [15] Space Telescope Science Institute. *JWST Propulsion*. URL: <https://jwst-docs.stsci.edu/jwst-observatory-hardware/jwst-spacecraft-bus/jwst-propulsion>.
- [16] Maamar Guendez Nassir Chellou and Abdallah Benarous. *Cooling of the Vulcain Nozzle's Divergent Wall*. URL: <https://pdfs.semanticscholar.org/81ca/2b1b18e058eb8229aaebd4f3e7804c738e64.pdf>.



- [17] Marco Pizzarelli. *Regenerative cooling of liquid rocket engine thrust chambers*. URL: https://www.researchgate.net/publication/321314974_Regenerative_cooling_of_liquid_rocket_engine_thrust_chambers#fullTextFileContent.
- [18] Dale L. Hook Robert L. Sackheim James S. Bassichis. *Spacecraft Attitude and Velocity Control Thruster System*. URL: <https://patentimages.storage.googleapis.com/90/c2/76/1f1f0ad0a8f7d6/US6135393.pdf>.
- [19] D. D. Evans T. W. Price. *The Status of Monopropellant Hydrazine Technology*. URL: <https://ntrs.nasa.gov/api/citations/19680006875/downloads/19680006875.pdf>.



POLITECNICO

MILANO 1863

Prova finale di Propulsione Aerospaziale

Appendix A MATLAB Codes

A.A.: 2022-2023
Prof: Galfetti Luciano

Garghetti Andrea	10734647	Melchiorre Federico	10710428
Grandinetti Roberta	10713569	Miccoli Francesco Antonio	10782473
Juvara Matteo Giovanni	10726898	Miolo Tommaso	10755151
Marzolini Alessandra	10724764	Modelli Simone	10728962
Mazzotti Luca	10744992	Nuccio Gabriele	10730683



A MATLAB Codes

A.1 Solid Propellant

A.1.1 CEAM analysis

The following code was used to obtain the CEA outputs in Section 2.2.2

```
clear all;
close all;
clc;

set(groot, 'defaultTextInterpreter', 'tex')
set(groot, 'defaultAxesTickLabelInterpreter', 'tex')
set(groot, 'defaultFigureColormap', turbo(256));
set(groot, 'defaultAxesFontName', 'Palatino Linotype', ...
    'defaultTextFontName', 'Palatino Linotype');
set(groot, 'defaultSurfaceEdgeAlpha', 0.3);
set(groot, 'defaultLineWidth', 2);
set(groot, 'defaultFigureColor', [1; 1; 1]);
set(groot, 'defaultAxesColor', 'none');
set(groot, 'DefaultAxesFontSize', 15);

%% ADD CEA TO PATH

addpath(genpath('CEAM 1.0.0.0'))

%% CEA INPUT

% Problem data
booster.pCC = 64:-3:40; % Chamber pressure to compute, vector or ...
    % single value
booster.CEA.problemType = 'rkt';
booster.CEA.thermoChem = 'equilibrium';

% Nozzle, if you want to use expasion ratios use the first two lines and
% comment the other 2, if you want to use pressure ratios do the opposite
% booster.CEA.nozzleParam = 25:2:40; % Expansion ratios to compute, ...
    % vector or single value
% booster.CEA.nozzleDef = 'sup,ae/at';
booster.CEA.nozzleParam = 64:-3:40;
booster.CEA.nozzleDef = 'pi/p';

% Oxidizer
booster.oxidizer.name = 'NH4CL04 (I)';
booster.oxidizer.wtFrac = 68;

% Fuel
booster.fuel.name = 'HTPB';
booster.fuel.wtFrac = 14;
booster.fuel.hf = -58;
booster.fuel.formula{1,1} = 'C';
```



```
booster.fuel.formula{2,1} = 7.075;
booster.fuel.formula{1,2} = 'O';
booster.fuel.formula{2,2} = 0.223;
booster.fuel.formula{1,3} = 'N';
booster.fuel.formula{2,3} = 0.063;
booster.fuel.formula{1,4} = 'H';
booster.fuel.formula{2,4} = 10.65;

% Additive
booster.additive.name1      = 'AL(cr)';
booster.additive.name2      = 'Al2O3(a)';
booster.additive.wtFrac = 18;
booster.additive.wtFrac1 = 0.89 * booster.additive.wtFrac;
booster.additive.wtFrac2 = 0.11 * booster.additive.wtFrac;

%% CEA

for i=1:length(booster.pCC)

    booster.sim{1,i} = CEA('case', 'boosterProb', 'prob', ...
        booster.CEA.problemType, 'p,bar', booster.pCC(i), ...
        booster.CEA.thermoChem, booster.CEA.nozzleDef, ...
        booster.CEA.nozzleParam, ...
        'reac',...
        'ox', booster.oxidizer.name, 'wt%', booster.oxidizer.wtFrac, ...
        'fu', booster.fuel.name, booster.fuel.formula{1,1}, ...
            booster.fuel.formula{2,1}, booster.fuel.formula{1,2}, ...
            booster.fuel.formula{2,2}, booster.fuel.formula{1,3}, ...
            booster.fuel.formula{2,3}, booster.fuel.formula{1,4}, ...
            booster.fuel.formula{2,4}, 'wt%', booster.fuel.wtFrac, ...
        'fu', booster.additive.name1, 'wt%', booster.additive.wtFrac1, ...
        'fu', booster.additive.name2, 'wt%', booster.additive.wtFrac2, ...
        'end');

end

%% SAVE DATA

save("boosterCEAdata.mat", "booster");

%% PLOT
% To use plotCEA function:
% Input 1: cell array of CEA simulations (do not touch, done ...
% automatically)
% Input 2: vector of chamber pressures evaluated (declared above)
% Input 3: stationsFlag, if 1 the plots will have an x axis composed of:
% [chamber, throat, expansionRatiol, expansionRatio2, ...]
% if stationsFlag is 0 the x axis in the plot will be:
% [expansionRatiol, expansionRatio2, ...]

plotCEA(booster.sim,booster.pCC,0)
```



A.1.2 Grains configurations

The following code was used to obtain the dimensioning of the grain in Section 2.3.2, Section 2.3.3 and Section 2.3.4.

```
clear all;
close all;
clc;

set(groot, 'defaultTextInterpreter', 'tex')
set(groot, 'defaultAxesTickLabelInterpreter', 'tex')
set(groot, 'defaultFigureColormap', turbo(256));
set(groot, 'defaultAxesFontName', 'Palatino Linotype', ...
    'defaultTextFontName', 'Palatino Linotype');
set(groot, 'defaultSurfaceEdgeAlpha', 0.3);
set(groot, 'defaultLineWidth', 2);
set(groot, 'defaultFigureColor', [1; 1; 1]);
set(groot, 'defaultAxesColor', 'none');
set(groot, 'DefaultAxesFontSize', 15);

%% ADD CEA TO PATH

addpath(genpath('CEAM 1.0.0.0'))

%% CEA INPUT

% Problem data
booster.pCC = 60; % Chamber pressure to compute, vector or single value
booster.CEA.problemType = 'rkt';
booster.CEA.thermoChem = 'equilibrium';

% Nozzle, if you want to use expasion ratios use the first two lines and
% comment the other 2, if you want to use pressure ratios do the opposite
% booster.CEA.nozzleParam = 25:2:40; % Expansion ratios to compute, ...
    % vector or single value
% booster.CEA.nozzleDef = 'sup,ae/at';
booster.CEA.nozzleParam = 50;
booster.CEA.nozzleDef = 'pi/p';

% Oxidizer
booster.oxidizer.name = 'NH4CLO4(I)';
booster.oxidizer.wtFrac = 68;

% Fuel
booster.fuel.name = 'HTPB';
booster.fuel.wtFrac = 14;
booster.fuel.hf = -58;
booster.fuel.formula{1,1} = 'C';
booster.fuel.formula{2,1} = 7.075;
booster.fuel.formula{1,2} = 'O';
booster.fuel.formula{2,2} = 0.223;
booster.fuel.formula{1,3} = 'N';
booster.fuel.formula{2,3} = 0.063;
booster.fuel.formula{1,4} = 'H';
booster.fuel.formula{2,4} = 10.65;
```



```
% Additive
booster.additive.name1      = 'AL(cr)';
booster.additive.name2      = 'Al2O3(a)';
booster.additive.wtFrac = 18;
booster.additive.wtFrac1 = 0.89 * booster.additive.wtFrac;
booster.additive.wtFrac2 = 0.11 * booster.additive.wtFrac;

%% CEA SIMULATION

engine = CEA('case', 'boosterProb', 'prob', booster.CEA.problemType, ...
    'p,bar', booster.pCC, booster.CEA.thermoChem, ...
    booster.CEA.nozzleDef, booster.CEA.nozzleParam, ...
    'reac',...
    'ox', booster.oxidizer.name, 'wt%', booster.oxidizer.wtFrac, ...
    'fu', booster.fuel.name, booster.fuel.formula{1,1}, ...
        booster.fuel.formula{2,1}, booster.fuel.formula{1,2}, ...
        booster.fuel.formula{2,2}, booster.fuel.formula{1,3}, ...
        booster.fuel.formula{2,3}, booster.fuel.formula{1,4}, ...
        booster.fuel.formula{2,4}, 'wt%', booster.fuel.wtFrac, ...
    'fu', booster.additive.name1, 'wt%', booster.additive.wtFrac1, ...
    'fu', booster.additive.name2, 'wt%', booster.additive.wtFrac2, ...
    'end');

% Engine data
Tc = engine.output.eql.temperature(1);
R = 8.314/(engine.output.eql.mw(1) * 1e3);

dr = 0.0074;
Pc = booster.pCC * 1e5;
tb = 135;
m = 238e3;
dt = 0.1;
time = (0:dt:tb)';

rhoF = 1690;

cStar = engine.output.eql.cstar(1);

% Application of 2D loss coefficient
nozzle.alphaDiv = deg2rad(15);
nozzle.lambda = (1+cos(nozzle.alphaDiv))/2;

perf.Ve = engine.output.eql.mach(end) * engine.output.eql.sonvel(end) ...
    * nozzle.lambda;

% Pressure ratio
[~,~,~,~,eps] = ...
    flowisentropic(engine.output.eql.gamma(2),engine.output.eql.mach(end));

% Atmospheric pressure
altRange = linspace(0,20000,length(time));
[~,~,Patm,~] = atmosisa(altRange,extended=true);

%% GRAIN CONSTANTS

grain.vol = m/rhoF;
grain.rExt = 2.964/2;
```



```
%% PROGRESSIVE COMBUSTION - ROUND PORT

% Geometrical parameters
round.rIn = grain.rExt - dr*tb;
round.l = grain.vol / (pi*(grain.rExt^2-round.rIn^2));

% The port radius over time is
round.rFun = linspace(round.rIn,grain.rExt,length(time));
round.rFun = @(t) interp1(time,round.rFun,t);

% Mass flow rate
round.dm = rhoF*2*pi*round.rFun(time)*round.l*dr;

figure();
plot(time,round.dm,LineWidth=5);
grid minor
xlabel("Time [s]",Interpreter="latex",fontsize=40)
ylabel("Mass flow rate [kg/s]",Interpreter="latex",fontsize=40)

% Throat Area
round.At = cStar * max(round.dm) / Pc;

% Thrust by altitude and time
round.thrust = round.dm * perf.Ve + (Pc/booster.CEA.nozzleParam-Patm') ...
    * round.At * eps;

figure();
plot(time,round.thrust/1e6,LineWidth=5);
grid minor
xlabel("Time [s]",Interpreter="latex",fontsize=40)
ylabel("Thrust [MN]",Interpreter="latex",fontsize=40)

% Ct
round.cT_vec = round.thrust / (Pc * round.At);
round.cT = engine.output.eql.cf(end);

figure();
plot(time,round.cT_vec,LineWidth=5);
yline(round.cT,'--k',LineWidth=3,Interpreter="latex",Label= ...
    "$c_T^{(0E)}$",fontsize=35,LabelHorizontalAlignment="left")
grid minor
xlabel("Time [s]",Interpreter="latex",fontsize=40)
ylabel("Coefficient of thrust []",Interpreter="latex",fontsize=40)
legend("$c_T$",Interpreter="latex",fontsize=35,Location="best")

% Itot
round.itot = trapz(time,round.thrust);

% Isp
round.ispVec = round.thrust ./ round.dm / 9.81;
round.isp = engine.output.eql.isp(end);
figure();
plot(time,round.ispVec,LineWidth=5);
yline(round.isp,'--k',LineWidth=3,Interpreter= ...
    "latex",Label="$I_{sp}^{(0E)}$",fontsize=35)
```



```
grid minor
xlabel("Time [$s$]",Interpreter="latex",fontsize=40)
ylabel("Specific Impulse [$s$]",Interpreter="latex",fontsize=40)
legend("$I_{sp}$",Interpreter="latex",fontsize=35)
% Iv
round.ivVec = round.ispVec * rhoF;
round.iv = round.isp * rhoF;

%% CONSTANT COMBUSTION - STAR GEOMETRY

% Mean Burn Area
star.Ab_mean = mean(round.rFun(time)*2*pi * round.l);

% Number of tips, fixed value from literature
star.n = 7;

% Height percentage, star tip height percentage with respect to the ...
% central
% perforatio
star.hPercentage = 0.5;

% Star tip length
syms rPort
star.width = 2*rPort * sin(pi/star.n);
star.d = rPort * (star.hPercentage - (1 - cos(pi/star.n)) );
star.tipL = sqrt((star.width/2)^2 + star.d^2);

% Burn area
star.burningPerimeter_i = 2*star.tipL*star.n;
star.burningPerimeter_f = 2*pi*grain.rExt;

% Find initial port radius by imposing constant area
fun = matlabFunction(star.burningPerimeter_i - star.burningPerimeter_f);
star.Rin = fzero(fun,1);
star.Rtip = star.Rin * star.hPercentage;
clear rPort

star.burningPerimeter_i = matlabFunction(star.burningPerimeter_i);
star.l = star.Ab_mean / star.burningPerimeter_f;

% Mass flow rate
star.dm = rhoF * dr * star.Ab_mean;

% Throat Area
star.At = cStar * star.dm / Pc;

% Thrust by altitude and time
star.thrust = star.dm * perf.Ve + (Pc/booster.CEA.nozzleParam-Patm') * ...
star.At * eps;
figure();
plot(time,star.thrust/1e6,LineWidth=5);
grid minor
xlabel("Time [$s$]",Interpreter="latex",fontsize=40)
ylabel("Thrust [$MN$]",Interpreter="latex",fontsize=40)

%% REGRESSIVE COMBUSTION - MOONBURN GRAIN
```



```
moon.rp = round.rIn;
% moon.rc = 0.9990;
moon.rc = 0.8;

if grain.rExt-moon.rp-moon.rc < 0
    error("Dimension given for moonburn grain geometry are ...
        incompatible, please fix them!");
end
ttt = (grain.rExt+moon.rc)/0.0074;
time = 0:0.1:ttt;
% Atmospheric pressure
altRange = linspace(0,20000,length(time));
[~, ~, Patm, ~] = atmosisa(altRange,extended=true);

moon.rVec = linspace(moon.rp,grain.rExt+moon.rc,length(time));

moon.Ab = zeros(length(time),1);
% viscircles([0,moon.rc],grain.rExt,Color=[0.8500 0.3250 ...
    0.0980],LineWidth=3);
for i=1:length(time)

    [xout,yout] = circloc(0,moon.rc,grain.rExt,0,0,moon.rVec(i));
    if ~isnan(xout)
        [theta,rho] = cart2pol(xout,yout);
        if yout(1) > 0
            moon.Ab(i) = moon.rVec(i) * abs(theta(2)-theta(1));
        else
            moon.Ab(i) = moon.rVec(i) * (2*pi + theta(2)-theta(1));
        end
    else
        moon.Ab(i) = moon.rVec(i)*2*pi;
    end
    hold on;
    % viscircles([0,0],moon.rVec(i),"Color",'k','LineWidth',1);
    % plot(xout,yout,'o',MarkerSize=5,Color=[0 0.4470 0.7410]);
end
moon.l = grain.vol/(pi * (grain.rExt^2-moon.rp^2));
moon.Ab = moon.Ab * moon.l;

figure
plot(time,moon.Ab,LineWidth=4)
xlabel("Time [s]",Interpreter="latex",fontsize=40)
ylabel("Burn Area [m^2]",Interpreter="latex",fontsize=40)

moon.dm = rhoF*dr*moon.Ab;

% Throat Area
moon.At = cStar * max(moon.dm) / Pc;

% Thrust by altitude and time
moon.thrust = moon.dm * perf.Ve + (Pc/booster.CEA.nozzleParam-Patm') * ...
    moon.At * eps;
figure();
plot(time,moon.thrust/1e6,LineWidth=5);
```



```
grid minor
xlabel("Time [$s$]", Interpreter="latex", fontsize=40)
ylabel("Thrust [$MN$]", Interpreter="latex", fontsize=40)
```

A.1.3 Nozzle dimensioning

The following code was used for calculation of the nozzle dimensions (Section 2.5)

```
clear
close all
clc

%% Nozzle dimensioning - single-port configuration

% CEA data
p_cc = 60e5; % [Pa]
c_star = 1730.299; % characteristic velocity [m/s]
eps = 7.98;

D_max = 3; % from the literature

m_flow = 2659.2; % maximum mass flow

A_t = c_star*m_flow/p_cc;
A_e = A_t*eps;

alfa_conv = 45*pi/180;
alfa_div = 15*pi/180;

D_t = sqrt(4*A_t/pi);
D_e = sqrt(4*A_e/pi);

L_div = (D_e-D_t)/(2*tan(alfa_div));
L_conv = (D_max-D_t)/(2*tan(alfa_conv));
L_tot = L_div + L_conv;

lambda = (1+cos(alfa_div))/2;
```

A.2 Liquid Propellant

A.2.1 Liquid 1

The following code is used for calculating outputs in section Section 3.2.6 and Section 3.2.8

```
%% Combustion chamber dimensioning
L_min = 0.76;
L_max = 1.02;
L_car = (L_max+L_min)/2;
V_c = A_t * L_car;
L_c = V_c/A_c;
A_lat = pi*D_c *L_c;
```



```
%% INjection plate

Δ_p_inj = 0.1 * P_c; %Suppongo le perdite al 10% della pressione in ...
    camera di combustione
D_h = 0.00157;
c_d = 0.9;
A_h = pi * D_h^2/4;
A_h_ox = m_flow_ox/(c_d * sqrt(2 * rho_ox * Δ_p_inj));
n_ox = ceil(A_h_ox/A_h);
A_h_f = m_flow_f/(c_d * sqrt(2*rho_f * Δ_p_inj));
n_f = ceil(A_h_f/A_h);
n_inj = min(n_f,n_ox);
A_1h_ox = A_h_ox/n_inj;
D_1h_ox = sqrt(A_1h_ox * 4/pi);
A_1h_f = A_h_f/n_inj;
D_1h_f =sqrt(A_1h_f * 4/pi);
%% Injection plate angles
u_ox = c_d * sqrt(2 * Δ_p_inj/rho_ox);
u_f = c_d * sqrt(2 * Δ_p_inj/rho_f);

alpha_f = deg2rad(50);
alpha_ox = rad2deg(asin((m_flow_f * u_f) / (m_flow_ox * u_ox)) * alpha_f);

%% Helium pressurization system

Δ_p_feed = 50 * 1e3;%[Pa]
v_feed = 10; %[m/s]
Δ_p_dyn_ox = 1/2 * rho_ox * v_feed^2;
Δ_p_dyn_f = 1/2 * rho_f * v_feed^2;
P_tank_O2_f = P_c + Δ_p_dyn_ox + Δ_p_inj + Δ_p_feed;
P_tank_H2_f = P_c + Δ_p_dyn_f + Δ_p_inj + Δ_p_feed;

%% Helium
%P_he = P_tank

P_tank_f = (P_tank_O2_f + P_tank_H2_f)/2;
gamma_He = 1.66;
MM_He = 4; %[g/mol]

T_tank_f = 55; %[K];
T_tank_i = 90; %[K]
P_tank_i = P_tank_f * (T_tank_i/T_tank_f) ^ (gamma_He/(gamma_He-1));

toll = 0.02;
R_He = R/ (MM_He * 1e-3);

V_He = 0;
m_tank = [];
j = 1;
m_tank(j) = 0;
m_tank(j+1) = P_tank_f/ (R_He * T_tank_f) * (V_ox + V_f + V_He);
while abs((m_tank(j+1) - m_tank(j)) / (m_tank(j))) > toll
    V_He = m_tank(j+1)/P_tank_i * T_tank_i * R_He;
    m_tank = [m_tank P_tank_f/ (R_He * T_tank_f) * (V_ox + V_f + V_He)];
    j = j+1;
```



```
end

%% Preburner and turbine
v_e = 4283.5; %[m/s]

H_inf_H2 = 120e+6; %[J/kg]

T_GG = 875; %[K]
P_GG = 10.1e+6; %[Pa]

T_H2_inlet = -237 + 273.15;
P_H2_inlet = 18.45e+6;

m_GG_tot = 9.7; %[kg/s]
OF = 0.9;

R_H2 = R/(MM_H2*1e-3);
gamma_gc = 1.3677; %from CEA
Cp_gc = 8.0740e+3; %from CEA
nu_turb = 0.98; %hyphotised

Pot_O2_turb = 5.1e+6; %[W]
Pot_H2_turb = 14.1e+6; %[W]

OF_stech = 8;
m_GG_H2 = m_GG_tot / (OF + 1);
m_GG_O2 = m_GG_H2 * OF;

m_GG_H2_burned = m_GG_O2 / OF_stech;
m_GG_H2_unburned = m_GG_H2 - m_GG_H2_burned;

Pot_tot_turb = Pot_H2_turb + Pot_O2_turb;

Tf = T_GG - Pot_tot_turb/(nu_turb*m_GG_tot*Cp_gc);
Pf = P_GG*(Tf/T_GG)^(gamma_gc/(gamma_gc-1));

epsilon_GG = 32;
eps_GG2 = epsilon/epsilon_GG;

fun_GG = @(Ma) eps_GG2 - (1./ (Ma)).*((1+(gamma_gc - ...
    1)/2.*Ma.^2)/((gamma_gc+1)/2)).^((gamma_gc+1)/(2*(gamma_gc-1)));
Ma_GG = fzero(fun_GG, [1, 10]);
MM_GG = 3.83;
R_GG = (R/(MM_GG*1e-3));

GAMMA_gc = sqrt(gamma_gc*(2/(gamma_gc+1))^((gamma_gc+1)/(gamma_gc-1)));
A_t_GG = m_GG_tot *sqrt(R_GG*Tf)/(GAMMA_gc*Pf);
A_e_GG = eps_GG2 * A_t_GG;
fun_P_e_GG = @(Pe) 1/eps_GG2 - ...
    ((gamma_gc+1)/2).^(1/(gamma_gc-1)).*(Pe/Pf).^(1/gamma_gc) ...
    .*sqrt((gamma_gc+1)/(gamma_gc-1).*((1-(Pe/Pf)).^((gamma_gc-1)/gamma_gc)));
P_e_GG = fzero(fun_P_e_GG, [0, 1e+6]);
```



```
T_e_GG = Tf*(P_e_GG/Pf)^((gamma_gc-1)/gamma_gc);
v_e_GG = loss_coeff * Ma_GG * sqrt(gamma_gc*R_GG*T_e_GG);
Thrust_GG = m_GG_tot * v_e_GG + (P_e_GG - P_e)*A_e_GG;

T_cc = m_flow_p*v_e;
I_GG = (T_cc)/(g0*(m_flow_p+m_GG_tot));
I_GG_con_spinta = (T_cc+Thrust_GG)/(g0*(m_flow_p+m_GG_tot));
I_GG_con_spinta-I_GG;
```

A.2.2 Liquid 2

The following code is used for calculating the outputs in section Section 3.2.5, Section 3.2.3 and Section 3.3

```
clear all;
close all;
clc;

set(groot, 'defaultTextInterpreter', 'tex')
set(groot, 'defaultAxesTickLabelInterpreter', 'tex')
set(groot, 'defaultFigureColormap', turbo(256));
set(groot, 'defaultAxesFontName', 'Palatino Linotype', ...
    'defaultTextFontName', 'Palatino Linotype');
set(groot, 'defaultSurfaceEdgeAlpha', 0.3);
set(groot, 'defaultLineWidth', 2);
set(groot, 'defaultFigureColor', [1; 1; 1]);
set(groot, 'defaultAxesColor', 'none');
set(groot, 'DefaultAxesFontSize', 15);

%% PATH GENERATION

if isunix()
    CEApPath = "../CEAM 1.0.0.0/";
else
    CEApPath = "..\CEAM 1.0.0.0\";
end

addpath(genpath(CEApPath));

%% ENGINE DATA

engine.tb = 540;
engine.Pc = 115e5;
utils.g = 9.81;
utils.R = 8.3145;
utils.Rair = 287.2;
engine.eps = 58.5;
engine.of = 6.1;
engine.dmp = 320;
ox.dm = engine.dmp * (engine.of/(engine.of+1));
f.dmp = 1/(engine.of+1) * engine.dmp;
ox.m = ox.dm * engine.tb;
f.m = f.dmp * engine.tb;
```



```
f.rho = 71;
ox.rho = 1140;
ox.V = ox.m/ox.rho;
f.V = f.m/f.rho;

%% CEA

ceaOutout = ...
    CEA('problem','rocket','frozen','nfz',1,'p,pa',engine.Pc,'o/f', ...
engine.of,'sup,ae/at',engine.eps, ...
    'reactants','fuel','H2(L)', ...
    'oxid','O2(L)','end');

%% PERFORMANCES

% Data input from CEA simulation
perf.M = ceaOutout.output.froz.mach(end);
perf.Ve_i = ceaOutout.output.froz.sonvel(end) * perf.M;
perf.isp = ceaOutout.output.froz.isp(end);
perf.ispVac = ceaOutout.output.froz.isp_vac(end);
gamma = ceaOutout.output.froz.gamma(2);
perf.gamma = gamma;
perf.cS = ceaOutout.output.froz.cstar(1);
perf.cT_i = ceaOutout.output.froz.cf(end);
perf.Pe = ceaOutout.output.froz.pressure(end);
perf.Tc = ceaOutout.output.froz.temperature(1);
perf.Tt = ceaOutout.output.froz.temperature(2);
perf.Pt = ceaOutout.output.froz.pressure(2);

% Application of 2D loss coefficient
nozzle.alphaDiv = deg2rad(15);
nozzle.lambda = (1+cos(nozzle.alphaDiv))/2;

perf.Ve = perf.Ve_i * nozzle.lambda;

%% AREAS AND NOZZLE

nozzle.At = perf.cS * engine.dmp / engine.Pc;
nozzle.Dt = sqrt(4*nozzle.At/pi);
nozzle.Ae = nozzle.At * engine.eps;
nozzle.De = sqrt(4*nozzle.Ae/pi);

%% THRUST

% Time vector
time = 0:0.1:engine.tb;

% Atmospheric Pressure
altRange = linspace(0,30000,length(time));
[~,~,Patm,~] = atmosisa(altRange,extended=true);

% Thrust
perf.T = engine.dmp * perf.Ve + (perf.Pe - Patm) * nozzle.Ae;
```



%% PERFORMANCES 2

```
perf.cT = engine.dmp * perf.Ve / (engine.Pc * nozzle.At);
perf.itot = trapz(time,perf.T);
perf.ispVec = perf.T / engine.dmp / 9.81;
engine.rhoAve = (ox.m + f.m) / (ox.V + f.V);
perf.ivVec = perf.ispVec * engine.rhoAve;
perf.iv = perf.isp * engine.rhoAve;

%% AREAS AND NOZZLE

nozzle.Dt = sqrt(4*nozzle.At/pi);

machFun = @(m) 1./m .* (2/(gamma+1) .* (1 + (gamma-1)/2 .* m.^2)) .^ ...
((gamma+1)/(2*(gamma-1)));

nozzle.Ac = nozzle.At * machFun(0.2);
nozzle.Dc = sqrt(4*nozzle.Ac/pi);

nozzle.alphaDiv = deg2rad(15);
nozzle.alphaConv = deg2rad(45);
nozzle.lConv = (nozzle.Dc-nozzle.Dt) / (2 * tan(nozzle.alphaConv));
nozzle.Ae = engine.eps * nozzle.At;
nozzle.De = sqrt(4*nozzle.Ae/pi);
nozzle.lDiv = (nozzle.De-nozzle.Dt) / (2 * tan(nozzle.alphaDiv));
nozzle.r = [linspace(nozzle.Dc/2,nozzle.Dt/2,500), ...
linspace(nozzle.Dt/2,nozzle.De/2,2000)];
nozzle.areas = pi * nozzle.r.^2;
nozzle.longitudinalCoordinate = ...
[linspace(0,nozzle.lConv,500),linspace(nozzle.lConv,nozzle.lDiv,2000)];

%% ISOENTROPIC EXPANSION IN THE NOZZLE

guess = [linspace(0.2,1,500), linspace(1,5,2000)];

solveMachFun = @(m) machFun(m) - nozzle.areas / nozzle.At;

engine.mach = fsolve(solveMachFun,guess);

nozzle.areaRatios = machFun(engine.mach);

engine.temp = (1 + (gamma-1)/2 * engine.mach.^2).^-1 .* ...
ceaOutout.output.froz.temperature(1);

mu = 1.0698*1e-4;
Pr = 0.5512;
k_c = 15.3748*1e-3/1e-2;
engine.bartz.recoveryFactor = Pr^(1/3); %recovery factor

Twi = (-150) +273.15;

Tcc_adiabatic = engine.temp(1) * (1 + engine.bartz.recoveryFactor * ...
(ceaOutout.output.froz.gamma(1)-1)/2 * 0.2);
```



```
sWall = 1.5e-3; %wall thickness
K_copper= 390; %[W/m*K]
engine.bartz.cpProducts = ceaOutout.output.froz.cp(2) * 1e3;

engine.bartz.sigma = @(Tw) 1./(( 1/2 * Tw/engine.temp(1) .* ...
    (1+(gamma-1)/2 .* engine.mach.^2) + 1/2 ).^ (0.8-0.6/5) .* ...
    (1+(gamma-1)/2 * engine.mach.^2).^(0.6/5));

h = @(Tw) ( (0.026/nozzle.Dt^0.2) * ...
    ((mu^0.2*engine.bartz.cpProducts)/Pr^0.6) * ...
    (engine.Pc/ceaOutout.output.froz.cstar(end))^0.8 ) .* ...
    (1./nozzle.areaRatios).^0.9 .* engine.bartz.sigma(Tw);

qWall = @(Tw) K_copper / sWall * (Tw-Twi);

eq = @(Tw) h(Tw) .* (Tcc_adiabatic-Tw) - qWall(Tw);

guess = 300 * ones(1,length(nozzle.areaRatios));

Twall = fsolve(eq,guess);

%% PLOTS and EXPORT

% Regenerative cooling
figure();
plot(nozzle.longitudinalCoordinate,Twall,'LineWidth',5)
ylabel("\textbf{Inside wall Temperature ... [K]}",Interpreter="latex",FontSize=40);
xlabel("\textbf{Longitudinal coordinate ... [m]}",Interpreter="latex",FontSize=40);
xline(2.5133,'k--',Label="End of regenerative ... cooling",Interpreter="latex",FontSize=20,LineWidth=3)

yyaxis right
plot(nozzle.longitudinalCoordinate,nozzle.r,'LineWidth',5)
ylabel("\textbf{Nozzle radius [m]}",Interpreter="latex",FontSize=40);

legend("Twall",FontSize=35)
axis padded
grid minor
title("Regenerative cooling");

% Thrust and Pressure over time
figure();
plot(time,perf.T,'LineWidth',3)
xlabel("\textbf{Time [s]}",Interpreter="latex",FontSize=20);
ylabel("\textbf{Thrust [N]}",Interpreter="latex",FontSize=20);
hold on

yyaxis right
plot(time,Patm,'LineWidth',3);
ylabel("\textbf{Ambient Pressure [Pa]}",Interpreter="latex",FontSize=20);

legend("Thrust")
```



```
axis padded
grid minor
title("Thrust and Pressure over time");

% Plot
figure();
plot(time,perf.ispVec, 'LineWidth',3)
yline(perf.isp, 'k--', 'LineWidth',2);
xlabel("\textbf{Time [s]}",Interpreter="latex",FontSize=20);
ylabel("\textbf{Specific Impulse [s]}",Interpreter="latex",FontSize=20);

yyaxis right
plot(time,Patm, 'LineWidth',3);
ylabel("\textbf{Ambient Pressure [Pa]}",Interpreter="latex",FontSize=20);

legend("Specific Impulse","OE Specific ...
    Impulse","AutoUpdate","off",'Location','best');
axis padded
grid minor
title("Specific Impulse and Pressure over time");

% Mach number
figure();
plot(nozzle.longitudinalCoordinate,engine.mach, 'LineWidth',2)
ylabel("\textbf{Mach [-]}",Interpreter="latex",FontSize=20);
xlabel("\textbf{Longitudinal coordinate ...
    [m]}",Interpreter="latex",FontSize=20);

yyaxis right
plot(nozzle.longitudinalCoordinate,nozzle.r, 'LineWidth',2)
ylabel("\textbf{Nozzle radius [m]}",Interpreter="latex",FontSize=20);

legend("Mach")
axis padded
grid minor
title("Mach number");
```